THE INFLUENCE OF METAL GRAIN STRUCTURE ON THE ATTENUATION OF AN ULTRASONIC ACOUSTIC WAVE

Thesis by

Robert Kenneth Roney

In Partial Fulfillment of the Requirements

For the Degree of

Doctor of Philosophy

California Institute of Technology

Pasadena, California

1950

ACKNOWLEDGEMENTS

The writer wishes to express his gratitude to Professor F. C. Lindvall, who suggested this research, and under whose patient direction it was conducted. He is additionally indebted to Professor D. S. Clark and Professor W. R. Varney for their generous advice and assistance in the metallurgical phases of this work, and for the use of the essential metallurgical equipment made available by Professor Clark.

Further appreciation is expressed to all those members of the staff with whom association has been a privilege and an inspiration in this and other endeavors.

ABSTRACT

Apparatus is described for the study of the propagation of ultrasonic acoustic waves in solid bodies and its applications in metallurgy. In particular, the anisotropy of attenuation in cold worked aluminum and the effect of anneal are demonstrated. Reflections from individual crystal faces are identifiable in bodies with average grain diameter of 0.17 mm. A critical discussion is given of a theoretical effect of grain size on wave attenuation as advanced by Mason and McSkimin[9], and an empirical relation reported by Roth[7]. The theory is extended to cover the complete range from that explored by Mason to that reported by Roth. Experimental deviation from the theoretical effect indicates other factors besides average grain size are effective in materials with asymmetrical grain structure.

Table of Contents

THE INFLUENCE OF METAL GRAIN STRUCTURE ON THE ATTENUATION OF AN ULTRASONIC ACOUSTIC WAVE

I. Introduction

The use of sound waves in numerous engineering applications and scientific research has experienced very rapid growth in the past decade. This growth was given marked impetus by the late war, with the search for underwater signalling devices, and with the development of means of generating and detecting these waves by electronic techniques associated with radar. The subsequent engineering applications have been largely for the purpose of metal interior investigations, for detecting and locating gross flaws, cracks, or inclusions in ingots, castings, or formed parts, or for determining the thickness of plates or sheets with one inaccessible surface[1,2,3,4,5]. For these purposes either the reflections of individual packets of waves may be observed and timed, or a continuous wave may be used to establish a resonance. But in general the frequencies used have been less than five megacycles per second, though frequencies as high as fifteen megacycles per second have been used in commercial equipment for inspecting the light alloys in which the damping of the waves is small[1]. An entirely different application has been the development of acoustic delay lines[6], particularly in digital computer applications. Here, advantage is taken of the relatively low propagation

velocity, compared to that of electrical signals, to construct compact delay networks of a few hundred microseconds delay and with sufficient band width to preserve pulses of a fraction of a microsecond rise time.

In all of these applications, a basic limitation arises in the natural damping or attenuation of the acoustic waves. For materials testing, increased frequencies or shorter wave lengths are desired in order to improve sensitivity to small objects, and to make possible shorter pulses for higher resolution. However it is found that in most solid materials attenuation increases rapidly with frequency, and the total attenuation or damping varies widely from one material to another. Further, great variation may occur in the damping in samples of the same composition but differing in heat-treatment or physical working histories. This behavior not only arouses interest in the nature of attenuation processes, but necessitates a better understanding of the mechanisms of the phenomena in order to establish the basic limitations and possibilities of a valuable tool. Further, the dependence of attenuation on the crystalline condition of the medium suggests its application directly in metallurgical studies by measurement of relative attenuations. The research reported in this thesis represents an exploration of these possibilities, and the construction of apparatus for measurement of the ultrasonic propagation properties of certain materials.

II. Theory of Ultrasonic Attenuation in Solids.

(a) Preliminary Theory and Previous Work.

While, as mentioned above, considerable work has been done in engineering applications of ultrasonics little has been published on the attenuation in polycrystalline materials in controlled experiments in the megacycle range, though valuable contributions have been made by Roth[7] and Mason and McSkimin[8,9,10], who investigated the frequency dependence of the attenuation constant, α. α is defined by the equation

$$I = I_o e^{-2\alpha x} \tag{1}$$

where I is the wave intensity* (power) at distance x, and I_o is the intensity at $x = 0$. That is, α is the logarithmic decrement. The theoretical variation of α with frequency will depend heavily upon the mechanism of energy loss considered. At relatively low frequencies (less than one megacycle per second) the Q** of solid materials has been observed by Wegel and Walther[11,10] to be practically constant for all frequencies within this range. Since this indicates a

---

* As used in this paper, if not specifically specified in other units, α defined in equation (1) is always in nepers per unit length. That is, if p_1/p_o is the ratio of wave amplitudes at $x = x_1$ and $x = 0$, respectively, then

$$\alpha x_1 = \log_e \frac{p_1}{p_o} = \frac{1}{2} \log_e \frac{I_1}{I_o} \quad \text{nepers.}$$

If specified in decibels, then,

$$\alpha x_1 = 20 \log_{10} \frac{p_1}{p_o} = 10 \log_{10} \frac{I_1}{I_o} \quad \text{db.}$$

** In general, Q of an oscillatory system may be defined in

constant per unit energy lost per cycle, it has been attributed to an elastic hysteresis effect. The Q thus observed for two materials of interest here are

Aluminum	Q = 10,000
Magnesium	5,700

At higher frequencies, or shorter wave lengths, other factors come into play, and the damping observed cannot be accounted for by extrapolation from values at lower frequencies, according to the above picture. Thus, working in the frequency range form 3 to 15 mc/sec, Mason and McSkimin[8] report an attenuation-frequency relation for a traveling dilation wave in duralumin 17S* alloy as follows:

$$\alpha = B_1 f + B_2 f^4 . \qquad (2)$$

$B_1 f$ represents the hysteresis damping as observed at lower frequency, and the second term is the additional damping not observed at lower frequency. On the basis of two specimens

---

terms of the ratio of the peak stored energy (whether electrical, magnetic, or mechanical strain energy) to the energy lost per cycle; thus, if energy loss is small,

$$\frac{\text{energy stored}}{\text{energy lost per cycle}} = \frac{Q}{2\pi}$$

Specifically, for a traveling wave, Q is defined,

$$Q = \frac{B}{2\alpha} = \frac{2\pi}{2\lambda\alpha} = \frac{\pi}{\lambda\alpha} ,$$

where B is the phase shift in radians per unit length, α the amplitude attenuation in nepers per unit length, and λ the wave length.

* The alloy designations used here in are the Alcoa commercial alloy designations.

tested varying nearly two to one in grain size (0.23 mm and 0.13 mm), but otherwise presumably identical, they concluded that the coefficients are,

$$B_1 \simeq \text{constant} = 0.65 \text{ to } 0.845 \times 10^{-9} \quad \text{neper/cm/cycle}$$

$$B_2 = kD^3 = 3.1 \times 10^{-25}(D^3) \quad \text{neper/cm/cycle}^4, \tag{2a}$$

where D is the grain diameter in millimeters. Since the Q of a rod is equal to

$$Q = \frac{B_o}{2A_o} = \frac{\text{Phase shift}}{2(\text{attenuation})} = \frac{2\pi l}{2\lambda\alpha l}, \tag{3}$$

we then can compute expected hysteretic damping extrapolated from low frequency,

$$\alpha_h = \frac{\pi}{\lambda Q} = \frac{\pi}{vQ} f = 0.497 \times 10^{-9} f \text{ neper/cm.} \tag{4}$$

The agreement with (2a) is seen to be fair. Combining the coefficients (2a) into equation(2), there results,

$$\alpha = B_1 f + kD^3 f. \tag{5}$$

This is quite in contrast with the relation reported by Roth[7]. Working with magnesium and aluminum, with grain sizes ranging from 0.2 to 2.0 mm and in the frequency range from seven to seventy megacycles, he reports

$$\alpha = 2 \times 10^{-9} \frac{f}{D} + k(D), \tag{6}$$

where K(D) is an undetermined function of D, but independent of f, and generally is small in comparison with the first term of (6).

Roth gives his equation only as an empirical fit to his observations. However Mason and McSkimin offer a very plausible theoretical explanation of their expression, though the range of applicability is very limited. Upon extension of the range of measurement to 30 megacycles[9], they observe a flattening off of the attenuation, and indeed approach an attenuation inversely proportional to particle diameter. They also attempt a reconciliation of their results with Roth's data, but not with the form of equation (6). The results of Roth and Mason as presented by those authors are sketched in Figure 1.

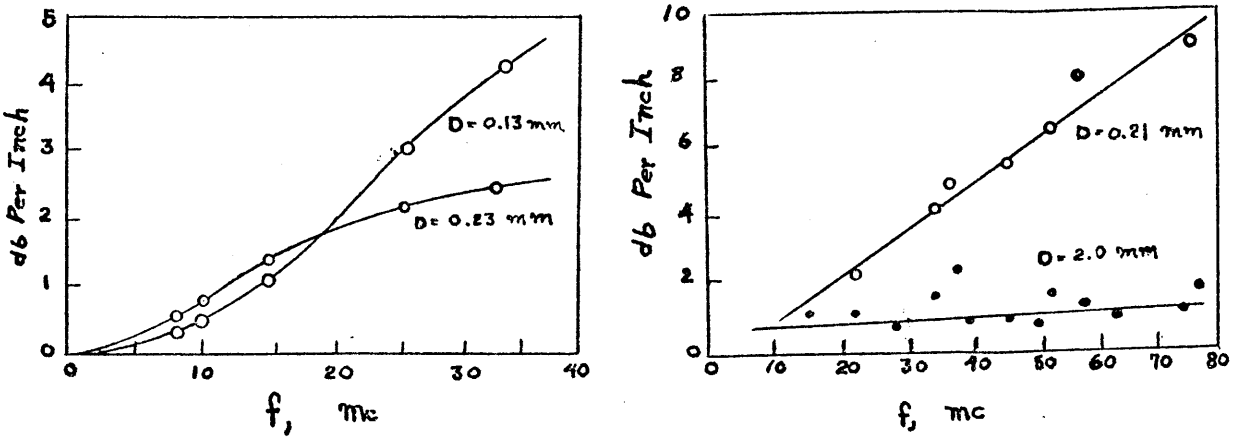

(a) Measured attenuation for dilation waves in duralumin alloy. (After Mason and McSkimin)

(b) Measured attenuation for dilation waves in magnesium. (After Roth)

FIGURE 1.

After a critical discussion of the derivation of equation (5) it will be shown that by a similar approach one can connect the existing data in a continuous and logical manner.

Polycrystalline metals such as form ordinary structural materials are composed of many separate and randomly oriented single crystals. In general, such a single crystal will exhibit different elastic properties along its various crystallographic axes, so that the elastic modulus in any direction may differ from the average. Accordingly, an acoustic wave encountering these discontinuities will undergo partial reflection or scattering in amounts depending upon the particle size, the elastic discontinuity, and the wave length of the radiation. Since the energy thus scattered is removed from the primary directed beam, the effect is quite the same as if the energy had been dissipated. In accounting for this effect, Mason and McSkimin[8] assume that for a limited frequency range, the well known Rayleigh[12] scattering law is valid, whereby the ratio of energy scattered by a particle of volume T to the energy incident upon its cross-section, A, is

$$\frac{W_S}{W_I} = \frac{4\pi^3 T^2}{A\lambda^4}\left[\left(\frac{\Delta\kappa}{\kappa}\right)^2 + \frac{1}{3}\left(\frac{\Delta\rho}{\rho}\right)^2\right] \qquad (7)$$

where λ, as before, is the radiation wave length, ρ the density and κ is the compression modulus (equal to c_{11} from the elastic tensor in solid bodies, for compression waves), all in the unperturbed medium, and $\Delta\rho$, $\Delta\kappa$ are the deviations

of density and compression modulus, respectively, for the scattering particle. Assuming $\Delta\rho = 0$, taking the number of particles as

$$N = \frac{A\,dx}{T} \tag{8}$$

and summing over all particles, neglecting multiple scattering, one obtains the familiar result,

$$\frac{1}{W_i}\frac{dW}{dx} = 2\alpha_s = \frac{4\pi^3 T}{\lambda^4}\left[\left(\frac{\Delta k}{k}\right)^2\right]_{ave} \tag{9}$$

where $(\Delta k/k)^2$ is averaged over all particles. It is shown that $\left[(\Delta k/k)^2\right]_{ave}$ for a cubic crystal is given by

$$\left[\left(\frac{\Delta k}{k}\right)^2\right]_{ave} = \left[\left(\frac{c_{11}' - \langle c_{11}'\rangle_{ave}}{\langle c_{11}'\rangle_{ave}}\right)^2\right]_{ave}$$

$$= \frac{4}{21}\left[\frac{\left[2\left(c_{12}-c_{11}\right)+4c_{44}\right]}{5c_{11}+2\left(c_{12}-c_{11}\right)+4c_{44}}\right]^2, \tag{10}$$

if all orientations of the crystals are equally probable. In equation (10), the primed quantities refer to the elastic tensor coefficients in any orientation, while the unprimed quantities refer to the same coefficients along the principal crystallographic axes. Hence $(c_{11}')_{ave}$ corresponds to the quantity

$$-\left(c_{11}'\right)_{ave} = \left(\lambda + 2\mu\right) = \frac{E(1-\varepsilon)}{(1+\varepsilon)(1-2\varepsilon)} \tag{11}$$

for an isotropic or polycrystalline medium, μ being the modulus of rigidity, λ Lamé's constant, E Young's modulus and

ε is Poisson's ratio.

Equation (9) gives the theoretical derivation of the second term of equation (5), now identified as the scattering component, by which the value of B in equation (2) becomes,

$$B_2 = \frac{2\pi^4}{3\lambda^4}\left[\overline{\frac{\Delta K}{K}}\right]^2 D^3. \qquad (12)$$

Table I lists the scattering factor $\left(\overline{\frac{\Delta K}{K}}\right)^2$ calculated for various metals of both the cubic and hexagonal crystal types. When the calculated value of $\left(\overline{\frac{\Delta K}{K}}\right)^2$ is used in equation (12), the resulting coefficient, B_2, is less than the empirical value, by a factor of about five. This is not surprising however, considering the sensitivity of the evaluation to the assumed diameter of the equivalent sphere of crystal grains.

TABLE I[10]

Metal	$\overline{(\Delta K/K)^2} \propto \left[\frac{C_{ij}' - \overline{C_{ij}'}}{\overline{C_{ij}'}}\right]^2_{ave}$	Propagation	Observer
Al	3×10^{-4}	good	Roth, Mason & McSkimin, Roney
Cu	7.4×10^{-3}	poor	Roth, Roney
Fe	6.8×10^{-3}	poor	Firestone, Roney.
W	0	very good	
Mg	2.2×10^{-4}	good	Roth, Mason & McSkimin
Cd	2.8×10^{-2}	very poor	Roney

Equation (5), or (9), is regarded by its authors as applicable for the range for which

$$D < \tfrac{1}{3}\lambda. \tag{13}$$

Serious exception is taken here to this condition on theoretical grounds, for it is in clear violation of the the requirement in Rayleigh's[12] original derivation that

$$\mu = \frac{\pi D}{\lambda} << 1. \tag{14}$$

If condition (14) is not met, higher order terms in μ are necessary.

Further objection to the above derivation has been made[7] because of the neglect of multiple scattering. The validity of the fourth-power law is well established for thinly dispersed scatterers, such as usually occur in the scattering of light, but the closely packed grains of a metal present a considerably different situation. However, it is felt that this is not a serious approximation, so long as $\overline{(\Delta k/k)^2}$ is indeed small, since any multiple scattering must be of higher order in this factor.

Despite its limitations, equation (9) or (12) is of value in indicating the importance of metallurgical condition and crystal elastic anisotropy in affecting damping. The propagation properties of various metals as indicated in Table I have been qualitatively verified both by the author and by other workers. For example, at frequencies above 20 mc/sec, penetration into iron and steel is limited to

a few millimeters, whereas at the same frequencies waves are detectable through several inches of aluminum without difficulty, in the proper metallurgical condition.

Mason has adopted a different mechanism to explain the attenuation in the region given by

$$D > 3\lambda, \tag{15}$$

in which he considers the wave amplitude loss at the separate crystal boundary surfaces, by use of the reflection coefficient. While his development[10] is more formal, it reduces basically to the following reasoning. In a highly directive wave train, energy may either be lost by normal reflection at a boundary, or by change of direction at oblique incidence, so that wave damping by this mechanism is a grain surface phenomena. Furthermore, the ratio of grain surface to grain volume is simply proportional to 1/D. Since the relative amplitude loss at normal reflection is the reflection coefficient, R, the attenuation is then

$$\alpha \simeq \frac{R}{D}, \tag{16}$$

and is likened to a diffusion process with mean free path D. By using certain assumptions, a quantitative result is obtained,

$$\alpha = \frac{2|R|}{D} \tag{17}$$

The reflection coefficient due to acoustic impedance discontinuity is[13]

$$R = \frac{Z_1 - Z_2}{Z_1 + Z_2} = \frac{\sqrt{c_{11}'\rho} - \sqrt{\bar{c}_{11}'\rho}}{\sqrt{c_{11}'\rho} + \sqrt{\bar{c}_{11}'\rho}} \approx \frac{1}{4}\left[\frac{c_{11}' - \bar{c}_{11}'}{\bar{c}_{11}'}\right]. \qquad (18)$$

An average value of R is estimated using the maximum and minimum values attained. By using this result, 1.6 db/inch attenuation is obtained for 2.0 mm grain-size magnesium, which agrees well with Roth's measurement in this region. However it is felt that this agreement is coincidental, for no account is taken for frequency dependent, or hysteresis losses, which alone would account for 1.0 to 1.4 db per inch, if the hysteresis constant does not decrease with frequency, and there is no evidence to indicate such occurrence. The principle considered seems reasonable, but this author objects to the use of the amplitude reflection coefficient, which may be either positive or negative, and in general confuses the primary issue of loss of energy. If instead, the power reflection coefficient is used, equation (17) for the amplitude attenuation constant becomes

$$\alpha_s = \frac{2\left(\frac{1}{2}\overline{R^2}\right)}{D} = \frac{\overline{R^2}}{D}$$

$$\text{total} \qquad \alpha = B_1 f + \frac{\overline{R^2}}{D} \qquad (19)$$

where R is, as before, the amplitude reflection coefficient and R^2 therefore is the power reflection coefficient. The subscript s indicates the scattering component of α.

Note that

$$\overline{R^2} \simeq \overline{\left(\frac{c_{\parallel}' - \overline{c_{\parallel}'}}{\overline{c_{\parallel}'}}\right)^2} = \left(\frac{\Delta k}{k}\right)^2 \qquad (19a)$$

that is, $\overline{R^2}$ is the same as the scattering factor used in equation (9). Just as in equation (9), the value of $\overline{(\Delta k/k)^2}$ taken from Table I results in an attenuation less than that actually observed.

At this point, no theory has been offered previously to connect the two regions discussed.

(b) Extension of the Theory.

In following an approach similar to that employed by Mason, but taking a slightly different point of view, it is possible to derive a theoretical explanation of results observed, extending over the complete range of frequencies and wave lengths discussed here. It may be observed that the apparent conflict between the observations and relations given by Mason and McSkimin on the one hand, and by Roth on the other hand is due to the manner in which the data are presented and the equations written. That is, the functions are written or plotted not in terms of the significant parameter, $\mu = \left(\frac{\pi D}{\lambda}\right)$, determining the type of phenomena occurring, but in terms of the dimensional components separately, πD, the particle circumference, and λ, the wave length.

In the following derivation, the major assumptions made are:

(a) That the total attenuation is a sum of a hysteretic

effect, α_H, and a scattering effect, α_s, throughout the range of interest.

(b) That the hysteresis constant for a given material remains constant for all frequencies considered.

(c) That when the scattered energy is sufficiently small, multiple scattering effects may be neglected, even in closely packed scatterers.

(d) That for uniform grain dimensions, and small elastic discontinuity, the total scattering effect may be approximated by the effect of the equivalent sphere.

All of these assumptions are valid in the Rayleigh fourth-power scattering region, though their rigor may be challenged outside this region.

The amount of energy scattered by a sphere in the path of a wave may be defined in terms of its scattering cross section, Q_s. Thus

$$W_s = Q_s \cdot I_i ,$$

where W_s is the scattered power, and I_i the incident intensity. Then, the ratio of scattered energy to the incident energy, or the attenuation per particle is, for a sphere,

$$\frac{dW}{W} = \frac{W_s}{I_i A} = \frac{Q_s}{A} = \frac{Q_s}{\pi\left(\frac{D}{2}\right)^2} . \qquad (20)$$

To get the attenuation constant, $2\alpha_s$, we must multiply by the number of particles per unit length,

$$2\alpha_s = \frac{dW}{W} \cdot \frac{1}{D} , \qquad \text{nepers/unit length,}$$

or,

$$\alpha_s D = \frac{dW}{2W} = \frac{1}{2}\frac{Q_s}{A} \quad \text{nepers.} \qquad (21)$$

For a rigid sphere, Morse[14] gives

$$\frac{Q_s}{A} = \frac{4}{\mu^2}\sum_{m=0}^{\infty}(2m+1)\sin^2\delta_m \qquad (22)$$

$$\xrightarrow[\mu\to 0]{} \frac{16}{9}\mu^4, \qquad \mu = \left(\frac{\pi D}{\lambda}\right) \qquad (22a)$$

δ_m is defined by the equation

$$\tan\delta_m = \frac{m\,j_{m-1}(\mu) - (m+1)\,j_{m+1}(\mu)}{m\,n_{m-1}(\mu) - (m+1)\,n_{m+1}(\mu)}, \qquad (22b)$$

and j and n are the spherical Bessel and Neumann functions. The form of Q_s/A is sketched in Figure 2. Rayleigh[12] shows that for a non-rigid sphere, at least for small values of μ, equation (22) is modified as

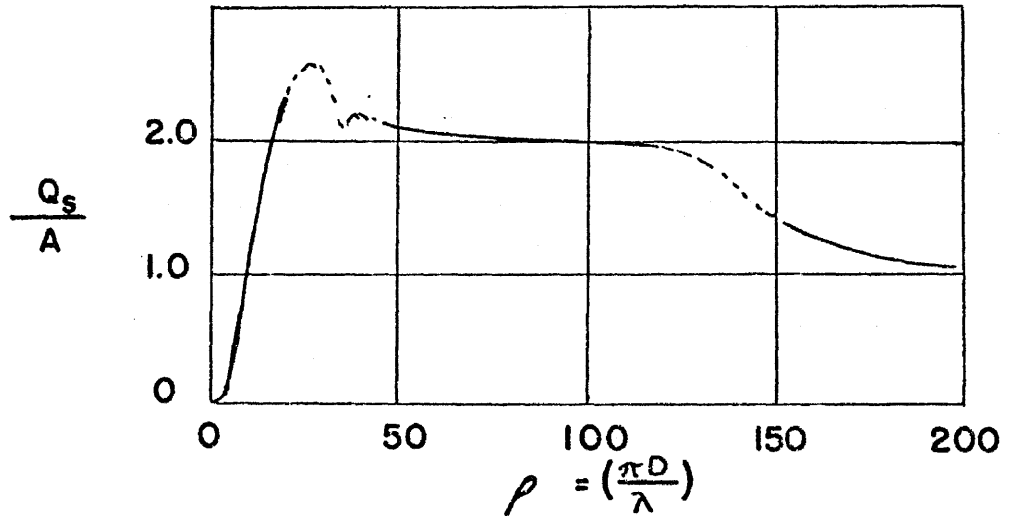

FIGURE 2.

$$\left.\frac{Q_s}{A}\right|_{\text{non-rigid}} = \left.\frac{Q_s}{A}\right|_{\text{rigid}} \times \left(\frac{\Delta k}{k}\right)^2 = \frac{4}{\mu^2}\left(\frac{\Delta k}{k}\right)^2 \sum_{m=0}^{\infty} (2m+1)\sin^2\delta_m \qquad (23)$$

or,
$$\left.\frac{Q_s}{A}\right|_{\text{non-rigid}} \xrightarrow[\mu \to 0]{} \frac{16}{9}\left(\frac{\Delta k}{k}\right)^2 \mu^4 \,, \qquad (23a)$$

where Δk is the increment of elastic modulus of the scatterer, and k the modulus of the unperturbed medium. It is again assumed that there is no density discontinuity. Equation (23a) corresponds to (7) of the previous section.
In what follows, the approximation is made that the modification in (23) is valid for the whole range of μ.

The attenuation due to hysteresis may be written

$$\alpha_H = B_1 f = \frac{B_1 v}{\lambda} = B_1' \frac{\pi}{\lambda} \,, \qquad (24)$$

or
$$\alpha_H D = B_1'\left(\frac{\pi D}{\lambda}\right) = B_1' \mu \,. \qquad (24a)$$

Combining (23), (24a), and (21),

$$\begin{aligned} \alpha D &= (\alpha_H + \alpha_S) D \\ &= B_1'\mu + \frac{2}{\mu^2}\overline{\left(\frac{\Delta k}{k}\right)^2} \sum_{m=0}^{\infty} (2m+1)\sin^2\delta_m \quad \text{nepers,} \end{aligned} \qquad (25)$$

we have a dimensionless equation in terms of the attenuation per particle diameter and the ratio of particle circumference to wave length. Let us inspect its behavior at the limits of the parameter μ. First, as $\mu \to 0$, by (23a),

$$\begin{aligned} \alpha D &\to B_1'\mu + \frac{8}{9}\overline{\left(\frac{\Delta k}{k}\right)^2}\mu^4 \\ &= B_1 D f + \frac{8}{9}\overline{\left(\frac{\Delta k}{k}\right)^2}\frac{\pi^4 D^4}{\lambda^4} \end{aligned}$$

or
$$\alpha = B_1 f + \frac{8}{9}\overline{\left(\frac{\Delta k}{k}\right)^2}\frac{\pi^4}{\lambda^4} D^3 f^4 . \qquad (26)$$

Compare equation (26) with (2) and (12). When $\mu \to \infty$, we have the case of geometrical shadow and for a rigid sphere,

$$\frac{Q_s}{A} \xrightarrow[\mu \to \infty]{} 1 \quad .$$

Then,

$$\alpha D \xrightarrow[\mu \to \infty]{} B_1' \mu + \frac{1}{2}\overline{\left(\frac{\Delta k}{k}\right)^2} \quad ,$$

or

$$\alpha \longrightarrow B_1 f + \frac{1}{2}\overline{\left(\frac{\Delta k}{k}\right)^2}\frac{1}{D} \quad . \tag{27}$$

Compare equation (27) with (19) and (19a).

Equation (25) is computed and plotted (αD as a function of μ) in Figure 3. The original data of both Roth and Mason and McSkimin are put in form of the dimensionless parameters and plotted with the computed curve. Instead of using the values of B_1, B_2, or $\overline{\left(\frac{\Delta k}{k}\right)^2}$ determined by Mason, the value of B_1 as computed from the low frequency Q, equation (4), was taken. A value of $\overline{\left(\Delta k/k\right)^2}$ was then chosen to give the best initial slope through the datum points for aluminum. The resulting scattering coefficient is

$$\overline{\left(\frac{\Delta k}{k}\right)^2} = 36 \times 10^{-4}, \tag{28}$$

as compared to 3×10^{-4} from Table I, and 15×10^{-4} computed from Mason's empirical value of B_2. With numerical coefficients, equation (25) then becomes,

$$\alpha D = 8.7 \times 10^{-4} \mu + \frac{6.29 \times 10^{-2}}{\mu^2} \sum_{m=0}^{\infty} (2m+1) \sin^2 \delta_m \, . \tag{28a}$$

The fit to the experimental data appears remarkable,

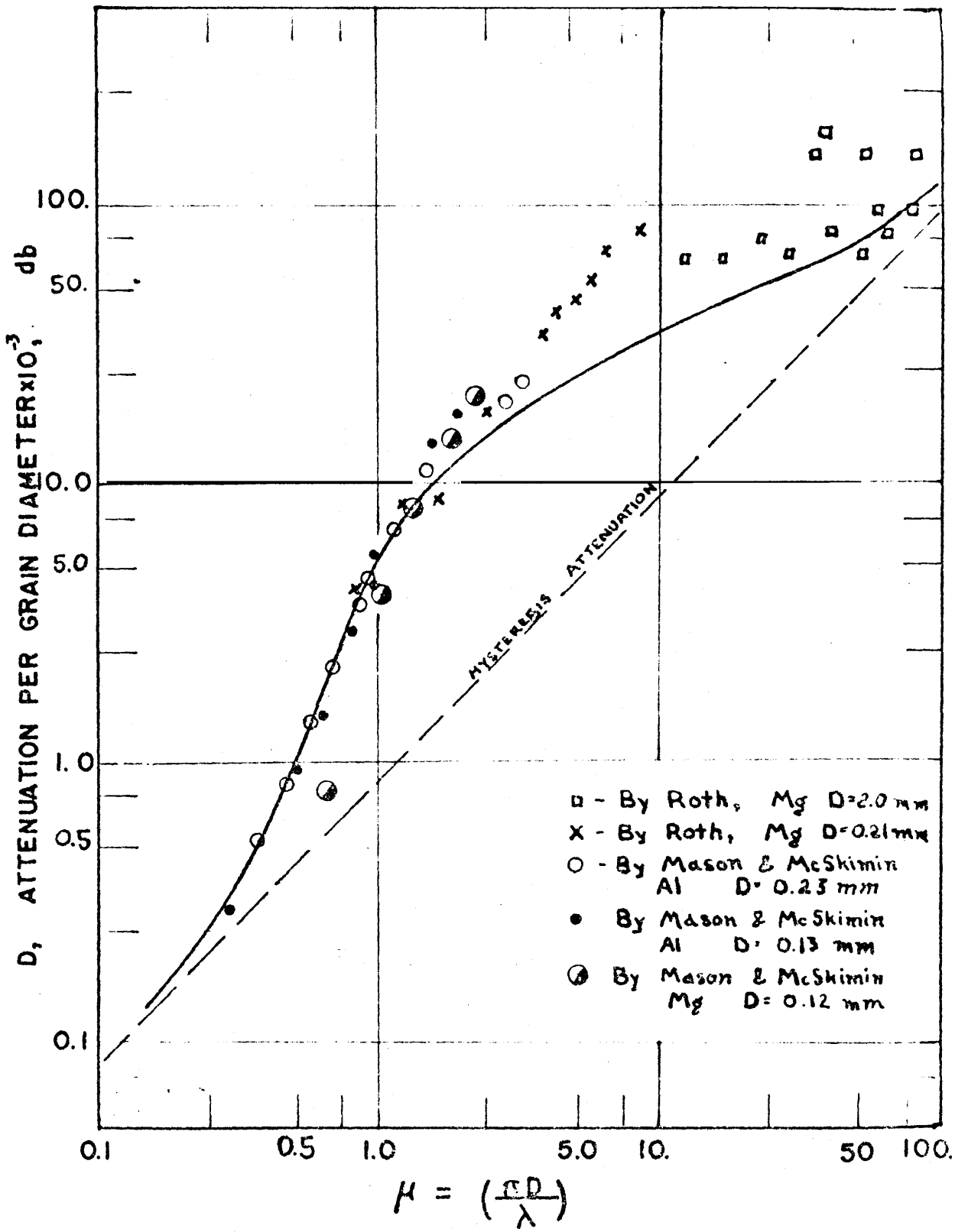

FIGURE 5. Plot of equation (55) or (20a), with the experimental data of Roth and Mason superimposed for comparison. The dashed line is the first term only of (55).

even though two different substance are involved. Of course such success could not be expected if the Q's and scattering factors were not similar for the two metals.

Even where the curve does not fit the data closely, the consistency and continuity of the various runs indicate that the dimensionless parameters used are the critical parameters for which there is a unique functional relation.

III. Experimental Apparatus and Technique.

(a) The Experimental Problem.

In view of the incomplete and somewhat conflicting knowledge of the fundamental processes involved in the ultrasonic attenuation in solids in the megacycle range, it becomes difficult to formulate engineering applications to give reliable tests of the status of a material based upon these ultrasonic propagation properties. It was therefore considered desirable to counter-check previously reported results with slight variations on previous experiments, and to investigate other parameters not considered or not reported in those experiments, which may contribute to anomalous results, and which at the same time may have immediate engineering significance. The apparatus described was developed to perform these studies, as well as to make certain qualitative observations in metal inspections.

The major variation in procedure has been the maintenance of constant frequency for all tests, and concentration upon the dependence on grain size, or more directly, the state of anneal. Considering the apparent importance of crystal diameter and elastic anisotropy in scattering or otherwise attenuating a wave, it seems reasonable to expect that any preferred orientation or elongation of grains remaining in a solid would have an appreciable effect upon the propagation, dependent upon the direction of propagation relative to such elongation. Accordingly, arrangements

are made to propagate a wave in each of three mutually perpendicular directions in each specimen.

(b) General Arrangement and Parameters.

The pulse technique has been adopted for this work because of the simplification in the acoustic situation. In this system the waves are generated in short bursts of perhaps only a few cycles at the desired frequency, the bursts being repeated at an appropriate rate. The simplification arises from the fact that the various signal modes or reflections are time separated and hence do not interfere but may be separately indentified. Basically, the tests consist of excitation of a traveling ultrasonic wave in a specimen to be studied and observing its reflections from various discontinuities within the medium. Specifically, the wave amplitude is measured as a function of the distance traveled. The general arrangement is indicated by the block diagram, Figure 4. Its operation is as follows: The modulation generator sends a narrow voltage pulse to the transmitter and a synchronizing signal to the oscilloscope to start the time sweep. The transmitter generates a pulse (0.5 to 2.0 microseconds duration) of radio-frequency energy which is transmitted to a quartz transducer. The quartz serves to convert the electrical signal to a mechanical wave which is coupled to the specimen in the acoustic tank, and thence back to the transducer. One transducer serves both as a transmitter and receiver. The

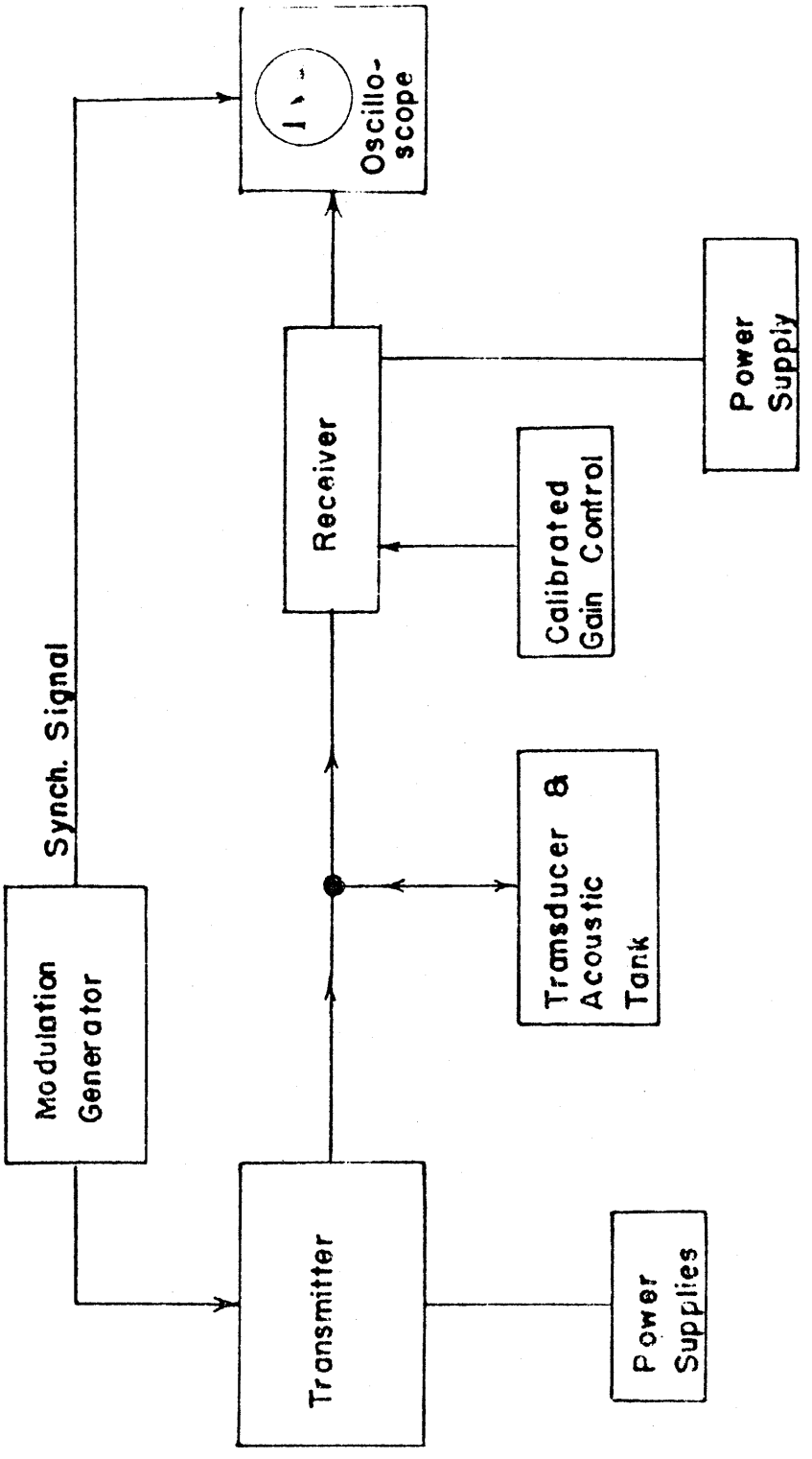

FIGURE 4. BLOCK DIAGRAM OF ELECTRICAL SYSTEM.

electrical signal from the transducer is displayed on the oscilloscope after amplification and detection by the receiver, where its amplitude is measured by means of the calibrated gain control.

A frequency of 30 mc/sec was chosen originally to be significantly above current commercial flaw detection equipment and yet to yield appreciable penetration in polycrystalline metals. Having chosen a frequency, the linear dimension of a single discontinuity required to give specular reflection will be of the order of the resulting wave length. For ready reference the velocities of dilation sound waves in several substances and the wave length at 30 mc/sec are listed in Table II.

TABLE II[13]

Substance	Velocity cm/sec	Wavelength, cm	inches
Water (25°C)	1.497×10^5	.00499	.00196
Aluminum	6.260×10^5	.0209	.00824
Iron	5.850×10^5	.0195	.00768
Cadmium	2.780×10^5	.00925	.00365
Copper	4.700×10^5	.0157	.00619
Mercury (20°C)	1.451×10^5	.00485	.00191

The resolution of successive reflections is limited by the pulse width. The minimum separation, a, that may be resolved is given by the equation

$$2d = v \Delta t,$$

where $v \cdot \Delta t$ is the distance traveled by the wave during the pulse interval Δt, and $2d$ is the round-trip distance between reflections. The pulse width or interval must be at least several wave periods and is limited not only by the transmitter output, but by the band-pass capabilities of the entire signal system.

(c) Electrical Components.

Of the electrical components, the transmitter and crystal matching networks require special attention. Chief requirements on the transmitter are; rapid rise and quench time of pulse, low noise generation during off-duty period, and high impedance to return signals. The requirement of rapid rise and quench time is particularly stringent for the relatively low carrier frequency of 30 mc/sec, with only 15 to 30 complete cycles in the pulse. These requirements are achieved with the circuit shown in Figure 5, which is an adaptation of a circuit used for radar simulator equipment by the MIT Radiation Laboratory(15). In this circuit, V2 and L1, along with the interelectrode capacitances of V1, V2, and V3 and trimmer C1, comprise a Hartley oscillator, with its grid loaded by the cathode impedance of V1. Vacuum tube V1 is normally heavily conducting through inductance L1, until interrupted by negative pulse from the modulation generator, which in this case is a standard laboratory pulse generator*. Cut-off of V1 causes the

---

* Model 79 B, Measurments Corporation, Boonton, N.J.

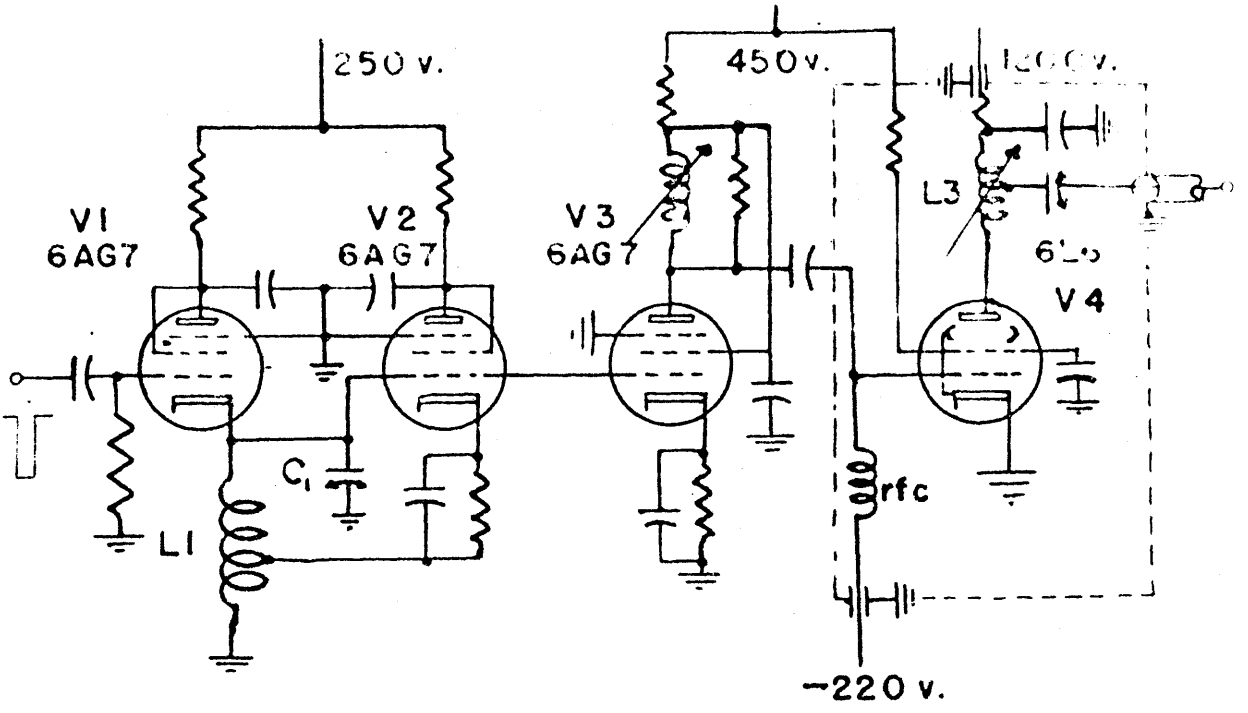

FIGURE 5. TRANSMITTER CIRCUIT.

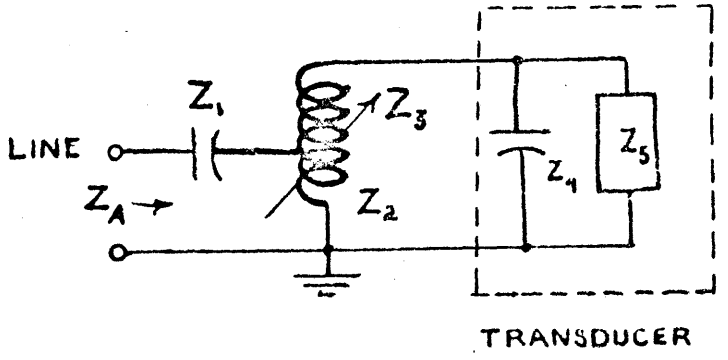

$$Z_2 + Z_3 + Z_4 = 0$$

$$Z_1 + Z_2\left(1 + \frac{Z_2}{Z_4}\right) = 0$$

$$Z_A = \left(\frac{Z_2}{Z_4}\right)^2 Z_5$$

FIGURE 6. HALF-WAVE MATCHING NETWORK.

tank circuit to ring, with a large initial amplitude. Upon reconduction of V1, the tank is heavily loaded and rapidly quenched.

It is important that the output stage be non-conducting during the off-duty, or listening period, if the receiver and transmitter are directly coupled, so that no emission noise from the transmitter is fed to the receiver first grid, since the receiver is operated at noise-limited sensitivity. Therefore the output stage is operated well in the class-C range.

An oscillogram of the transmitter output into a dummy load of 70 ohms (the line impedance) is shown in Figure 7. The pulse is seen to rise to full amplitude in about three RF cycles, and to decay in about five cycles. The decay time is somewhat prolonged by the quartz transducer, due to imperfect impedance matching over the broadband of the pulse.

In order that the transmitter will not accept any of the returned energy from the transducer, its output impedance, as seen from the line is made infinite by adjusting L3 to parallel resonance with the plate capacitance of V4 when not loaded by the g_m of V4, i.e. when V4 is not conducting.

A matching network for the crystal is equally important for efficient power transfer. The relatively large shunt static capacitance of the crystal and holder must be balanced out. Further, the equivalent shunt resistance is al-

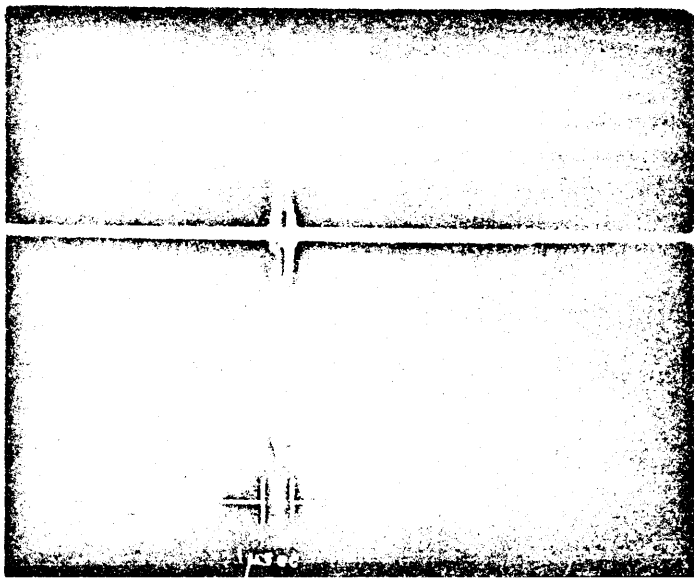

FIGURE 7. Out put pulse of transmitter, showing rapid rise and decay time.. Pulse consists of approximately 30 complete cycles.

ways high, even for a heavily acoustically loaded crystal, and must be transformed to the line impedance if the operation is to be independent of line length. The form of half-wave network used at both the transmitter and at the transducer is indicated in Figure 6.

(d) Acoustic Components.

In the present experiments, specimens being inspected were coupled to the transducer by means of a water bath. Figure 8 is a drawing of the acoustic system. A water bath is particularly suitable for rapid changing of many small specimens, but it requires special arrangement to align the specimen with the beam, as will be shown. This is accomplished by a vernier screw which rotates the tank and quartz crystal about a horizontal axis through the face of the specimen, and a second vernier adjustment on the specimen holder, Figure 9b, for alignment about a vertical axis. To facilitate rapid change of samples, they were mounted on the holder by sealing the polished face of the sample to the plane face of the holder with high vacuum grease. This proved quite satisfactory for light specimens.

The most important acoustic component is the transducer itself. The transducer is an x-cut quartz piezoelectric crystal, ground for a ten megacycle per second fundamental mode, but driven at its third harmonic. Since the electric field is along the x or electric axis, it oscillates in a piston mode and so generates compressional waves in the medium surrounding it. The area of the crystal must be a

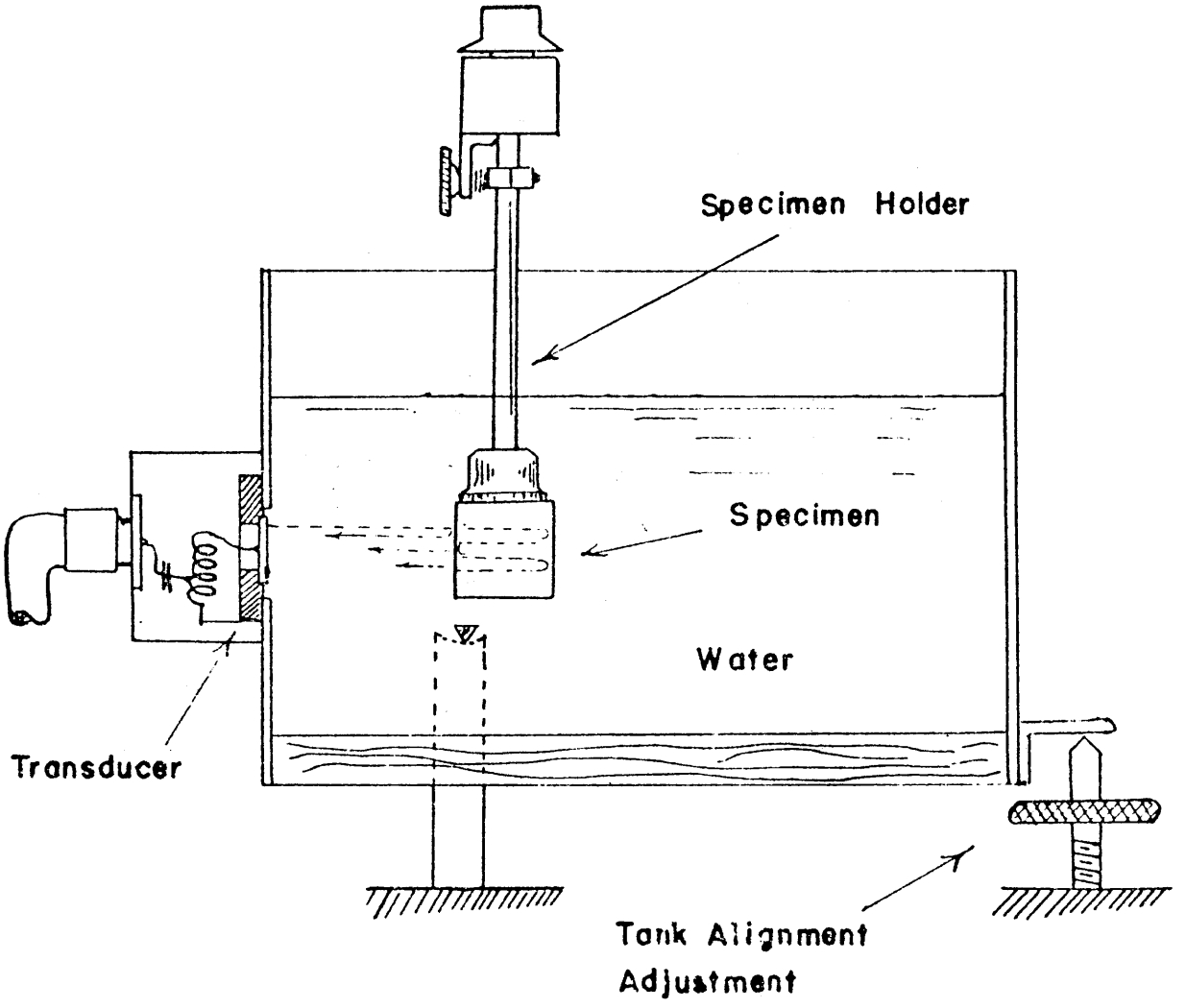

FIGURE 8. Sectional drawing of arrangement of acoustic components.

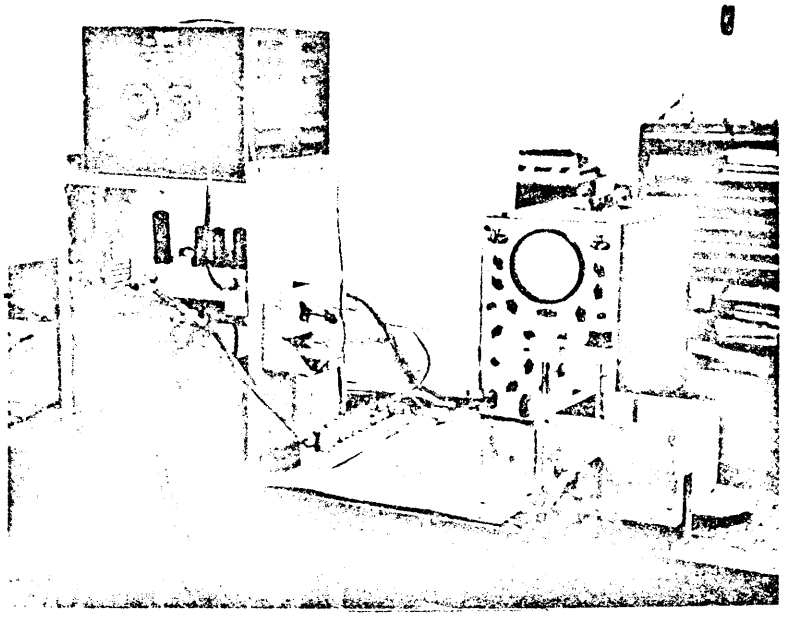

(a)

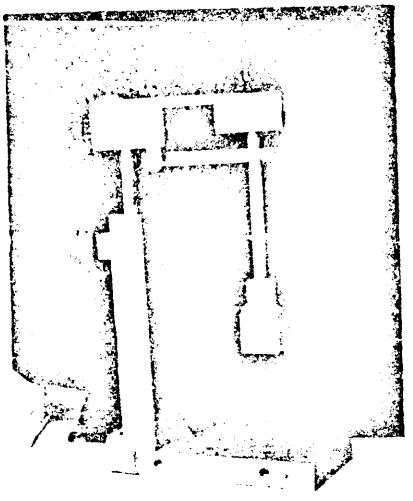

(b)

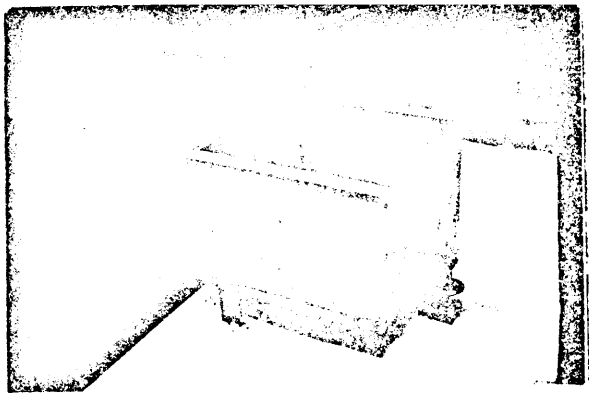

(c)

FIGURE 9. a. Photograph of overall apparatus.

b. Photograph of specimen holder with specimen attached.

c. Photograph of acoustic tank, showing means of alignment about horizontal axis.

compromise between the beam resolution or inspection area desired on the one hand, and the total available power and allowable beam divergence attenuation on the other hand. The design finally used has a circular active area of 1.542 square centimeters, or a diameter of 1.40 cm. A glance at Table II shows that this is 280 wave lengths in water, hence the wave beam pattern in water in the Fraunhofer diffraction region, as given by the equation,(14)

$$\frac{I}{I_0} = \left[\frac{2\,J_1(\mu \sin\theta)}{\mu \sin\theta}\right]^2, \qquad (29)$$

$$\mu = 2\pi a/\lambda = 280\pi, \qquad (29a)$$

gives a first zero at the half angle

$$\theta = 0.00436 \text{ radians}$$

$$= 0.25^\circ .$$

The second maximum, at 0.46°, is down by 36 db. It is seen, therefore, that the beam remains quite confined. This is borne out experimentally, with measurements indicating that the beam remains within the 1.4 cm diameter of the transducer, within the limits of the tank. Actually, the attenuation measurements are taken within the Fresnel diffraction region, so that divergence attenuation is indeed negligible.

One of the most important technical problems associated with the design of a quartz transducer is damping its naturally very high Q. This is most effectively accomplished

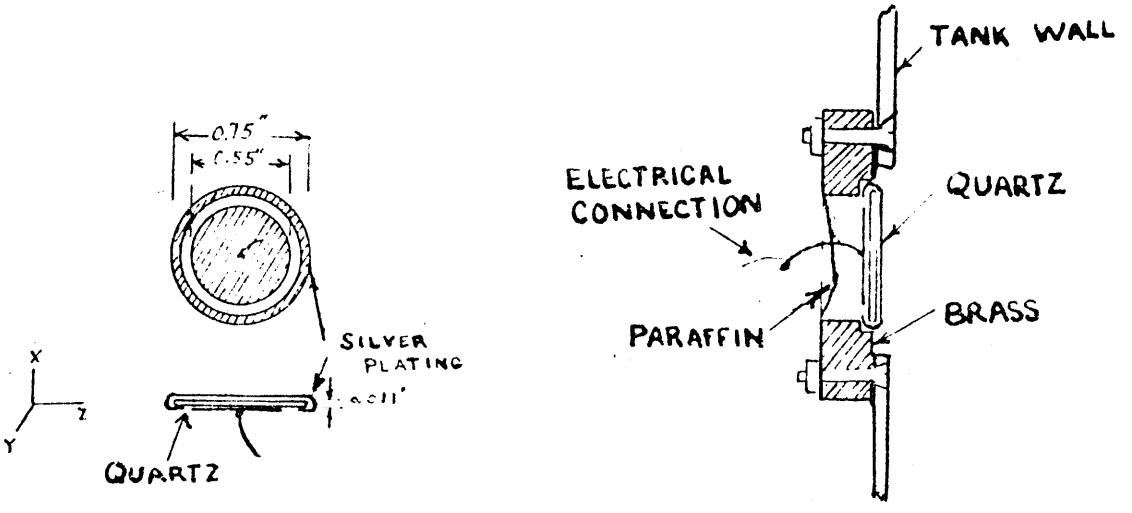

(a) (b)

FIGURE 10. Transducer Design.
(a) Shows the dimensions and plating of the x-cut quartz.
(b) Shows the mounting and damping method.

mechanically. Even when loaded on one side with water, the crystal rings at sufficient amplitude to saturate the receiver for about 100 microseconds after excitation by a 600 volt, 1 microsecond pulse of RF energy. After considerable experimentation the design shown in Figure 10 was found to be satisfactory. The crystal is silver plated on each side, with an annular ring separating the two electrodes on the back surface. The crystal is soft-soldered into a brass block, with the space behind the quartz filled with paraffin wax, cast in place. This was found to be more effective than cementing the quartz to bakelite or micarta of comparable thickness, as recommended by some workers[1]. The bakelite serves to load the crystal quite effectively, but as many as two or three reflections from the back surface of the bakelite were observed. This is partially prevented in the paraffin load used here by the concave shape of the meniscus of paraffin, serving to scatter the reflected wave.

The overall performance of the system is indicated by Figure 11, which shows the reflection from an 0.005 inch copper wire suspended in the water at distance of 2.5 inches from the transducer. The pulse on the left is the transmitter pulse. Even at the high receiver gain setting of this picture, the ringing of the transducer is seen to only slightly outlast the recovery of the receiver.

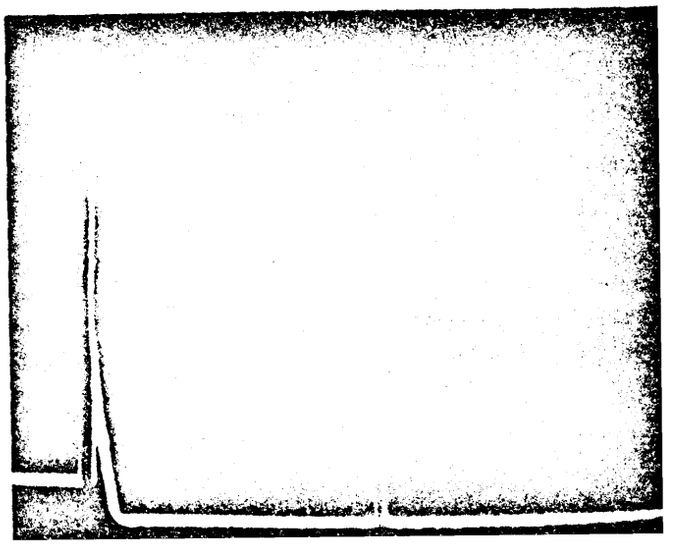

(a)

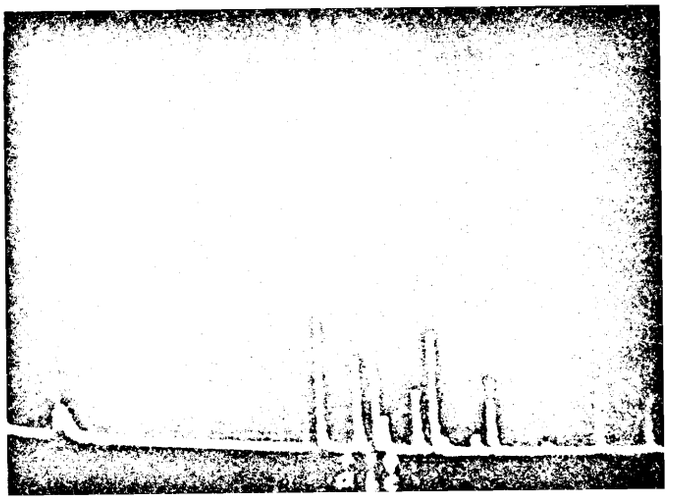

(b)

Figure 11. a. Performance of system, showing the echo from a single copper wire of 0.005 inch diameter suspended in beam at 2.5 inches range from the transducer.

b. Echo from an 0.03 inch hole drilled into a two inch aluminum block. d is the reflection from the front surface of the specimen, b from the back surface, a from the hole. Echo c results from a reverberation of the wave from the rear surface, to the hole, back to the rear surface and thence to the transducer. The hole is located 3/8 inch from the rear surface.

(e) Measurement Technique. Special Precautions and Corrections.

A wave introduced into a specimen through the water bath is reflected back and forth between the surfaces, and the amplitude is measured each time it is reflected from the front-surface. Specimens are cut from the material to be tested in the form of cubes or rectangular prisms. Opposite sides must be accurately parallel and smooth. Due to the very narrow beam of the transducer, parallelism must be within

$$\beta < \frac{.009}{n} \text{ radians,}$$

where β is the angle between opposite sides, and n is the number of reflections. That this is true is shown in the following manner:

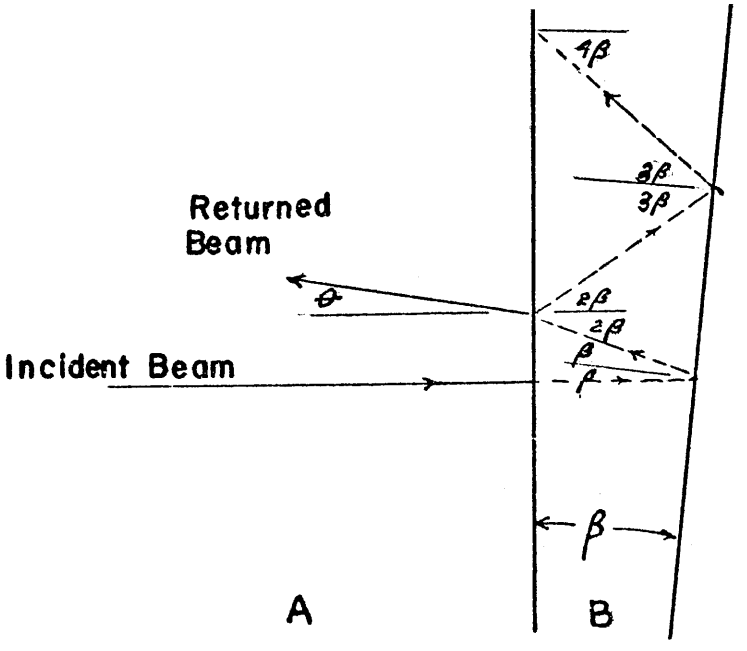

FIGURE 12.

In figure 12, the wave traveling inside medium B changes direction by angle 2β on each round trip, or $2n\beta$ for n round trips. The wave transmitted to medium A is refracted according to Snell's law, so that

$$\frac{\sin \theta_m}{\sin 2n\beta} = \frac{v_B}{v_A} \quad . \tag{30}$$

For the case of a water-aluminum interface, and since β and θ_m are small,

$$2n\beta = \frac{6.3}{1.5}\,\theta_m = 4.2\,\theta_m$$

But θ_m must be less than the half-angle beam width, or

$$\beta = (2.1/m)\,\theta_m < \frac{0.009}{n} \text{ radians.}$$

If this condition is not met, excessive attenuation will be indicated. By similar reasoning, the specimen as a whole must be carefully aligned with the beam.

At each reflection of the wave, energy is lost by transmission to the water. This requires a correction to the attenuation measured. The power reflection coefficient, R_p, is given by (13)

$$R_p = \left(\frac{Z_1 - Z_2}{Z_1 + Z_2}\right)^2 = \left(\frac{\rho_1 v_1 - \rho_2 v_2}{\rho_1 v_1 + \rho_2 v_2}\right)^2 \tag{31}$$

for normal incidence on an interface between infinite media. Here, Z_1 and Z_2 are the acoustic impedances of medium 1 and medium 2, respectively, and ρ and v are corresponding densities and velocities, as before. Thus after each reflection, the relative wave intensity is

$$\frac{I_n}{I_{n-1}} = R_p e^{-2\alpha d} = e^{-2\alpha' d}, \tag{32}$$

where d is the distance between reflecting surfaces, 2α is the power attenuation constant, and $2\alpha'$ is the apparent attenuation constant. Thus,

$$2\alpha = 2\alpha' - \frac{1}{d} \ln \frac{1}{R}. \tag{33}$$

Rewriting equation (31) as

$$R_p = \left(\frac{\frac{\rho_1 v_1}{\rho_2 v_2} - 1}{\frac{\rho_1 v_1}{\rho_2 v_2} + 1.} \right)^2, \tag{31a}$$

we see that only a measurement of relative density (specific gravity) and relative velocity are needed to compute R_p. In this case, a very simple arrangement is devised to measure velocity ratio. The water range of the specimen is varied until the n-th inner reflection exactly coincides with the second outer reflection occuring between the front surface and the quartz. Under this condition, if subscript 2 refers to the water,

$$\frac{nd}{v_1} = \frac{l}{v_2}$$

$$\frac{v_1}{v_2} = \frac{nd}{l},$$

where d is the block thickness, as before, and l is the water path length. These two quantities are easily measured to high precision. Reflection coefficients determined in this manner agree quite well with values measured by

Roth[7] by a different method;

Power Reflection Coefficient with Water:

Material	Roth	Roney
Aluminum (2S)	.708	0.704 ± ½%
Duralumin (24S)	---	0.711 ± ½%

Similarly, a comparison of velocity measurements may be made, where the author's relative velocity measurements are converted by the use of Bergmann's[13] value for the velocity in water (Table II).

Velocity of Compressional Waves (Units of 10^5 cm/sec):

Material	Roth[7]	Mason[8]	Roney	Bergmann[13]
Aluminum	6.31 ± .01	---	6.32 ± .06	6.26
Duralumin	---	6.32	6.32 ± .06	---

No particular care was taken to obtain accurate velocity measurements, since they did not appreciably affect the accuracy of attenuation measurements.

IV. EXPERIMENTAL PROCEDURE AND RESULTS.

While, from an engineering point of view, it would be desirable to make immediate application to steel, this was not attempted for two reasons, (a) the very low penetration at the frequencies of interest, and (b) the complicated structure, making it difficult to determine the effect of the many parameters. In addition it was desired to employ materials similar to those previously reported upon to facilitate comparison. For these reasons, two materials were investigated:

I. Commercially pure aluminum, 2S, not less than 99% Al.

II. Duralumin alloy, 24ST, Cu 4.4%, Mn 0.5% Mg 1.5%, Al not less than 92%.

In order to avoid possible variations in composition and previous history, all samples of each material were cut from a common stock. Since anisotropy of grain structure was particularly of interest, one inch rolled plate stock was selected for each case. The 2S aluminum was procured in the as-fabricated, cold rolled condition, giving very fine grain structure. Samples from each material were then given successive amounts of anneal as shown in Table III.

The ultrasonic propagation at 30 mc/sec was observed and the attenuation measured, when possible, in three normal directions in each sample. To facilitate reference these directions are designated as shown in Figure 13.

TABLE III

Sample No.	Temperature	Time in Minutes
2S Aluminum		
A	unannealed	
D	420° C	25
E	475° C	"
F	540° C	"
G	600° C	"
24S Duralumin		
1	unannealed	
2	350° C	5
4	420° C	30
5	500° C	"
6	560° C	"

Typical results of these observations are shown in the curves of Figures 14 and 15, and the oscillograms, Figures 21, 22, and 24 to 27. Figure 14 shows the echo amplitude, as measured, and without corrections applied, plotted against the number of reflections for duralumin samples, while Figure 15 gives a similar plot for the aluminum. Since the signal amplitudes are plotted on a logarithmic scale, a constant attenuation coefficient α results in a straight. line. Deviations from a straight line, greater than experimental error, indicates heterogeneous structure of the medium, or otherwise anomalous propagation. Such deviation

can result from imperfect alignment of the specimen in the beam. It may be noted that in most cases the data observed shows little deviation. A summary of the results for all samples, after correction for the reflection coefficient as described earlier, is given in curves of Figures 16, 17, 18, and 19, in terms of the temperature of anneal. In both the aluminum and the duralumin the scattering attenuation was so great in the samples of highest anneal that no quantitative measurements were possible. Since attenuations as high as 10 db/inch were readily measurable, it may only be inferred that the attenuation exceeded this amount. The estimated result is indicated in Figures 16 and 17 by the wavy line.

Note that the suspected anisotropic attenuation is indeed demonstrated to a remarkable degree in both materials. However the different behavior with anneal between the two materials is not readily explained. Whereas the aluminum shows less anisotropy as anneal is increased, the duralumin shows increased anisotropy. Reference to the metal structures as revealed in the micrographs, Figures 23 and 28, sheds some light on this question. Figure 28 shows that even with the great grain growth occurring in the duralumin, elipticity of the grains has not changed appreciably. On the other hand, the aluminum shows an early attainment of nearly uniform grains. In addition, it must be borne in mind that 24S duralumin is a heat-treatable alloy, and hence possesses multiple phases which play varying roles

in the heat-treat process, and may affect the acoustic properties quite separately form the grain scattering.

In connection with the anisotropic scattering attenuation, a very interesting observation can be made regarding the oscillograms, Figure 27(a,b,c); (a) shows the echo signal adjusted to observe the damped train of internal reflections, as well as a second external reflection and its train, observed for sample 4, with propagation in the x-direction. (b) shows a portion of the same signal expanded and the sensitivity increased ten-fold to observe reflections from the microstructure between the major surface reflections. (c) shows a signal under identical conditions as (b), for the same specimen, except that the propagation is in the z-direction. It is interesting to note that the large grain return is observed in the orientation for which the main wave attenuation is least (see Figure 18). A similar ultrasonic response is observe for sample no. 1. This is a rather surprising fact in view of the picture which we have established for the mechanism of major attenuation. The only explanation that is offered is that since the larger area faces of the grains are normal to the z axis, more of the scattered energy is directed back along the incident beam to the transducer, i.e,, scattered through 180^{o}, when the wave is propagating in the z-direction than when the propagation is normal to z, while the total scattered energy is no greater.

As mentioned earlier, the scattering in duralumin

sample 6 and aluminum sample G was so great as to make quantitative measurement impossible. This is shown in Figures 22 and 26. The large grain return completely masks any back surface reflection.

The actual attenuation constants measured are scattered so widely, as a function of orientation, that it is difficult to make any conclusions on the absolute magnitude of attenuation. In general it may be said that the attenuations measured average about twice those reported by Mason and McSkimin for the same conditions of $\pi D/\lambda$, and hence to that extent agree with reports by Roth on 2S aluminum. Unfortunately , insufficient range of grain diameter is achieved within measurable attenuation limits to indicate the relation of α to D . This is further limited by the inadequacy of etchants for the metallography of aluminum in revealing the microstructure of fine grain, unannealed aluminum. However the datum points obtained are placed on the generalized, dimensionless curve as derived in section II (b), and are shown in Figure 30. The actual ordinates of the two points farthest right are undetermined as indicated above, except that a lower limit may be set. On the other hand, while attenuation could be measured in samples A,D, 1, and 2, the grain size remains unrevealed by the microexamination (see for example Figure 28a). Hence the corresponding datum points can be plotted only as loci of possible positions. Each locus of αD as a function of $\pi D/\lambda$ on the double logarithmic scales is a straight line

of unity slope, with its vertical position determined by α. Accordingly, these loci are included on Figure 30 extending over the range of estimated limits of grain diamter for aluminum sample A and duralumin sample 1.

While the scatter of points seems extreme, it will be observed that the parameter μ lies in the range of maximum rate of change of αD. High sensitivity to grain ellipticity therefore is to be expected.

Duralumin shows less attenuation in the unannealed or hardened state than does commercial aluminum, but the sensitivity to heat treatment is higher for duralumin, the multiple phase alloy, than for pure aluminum.

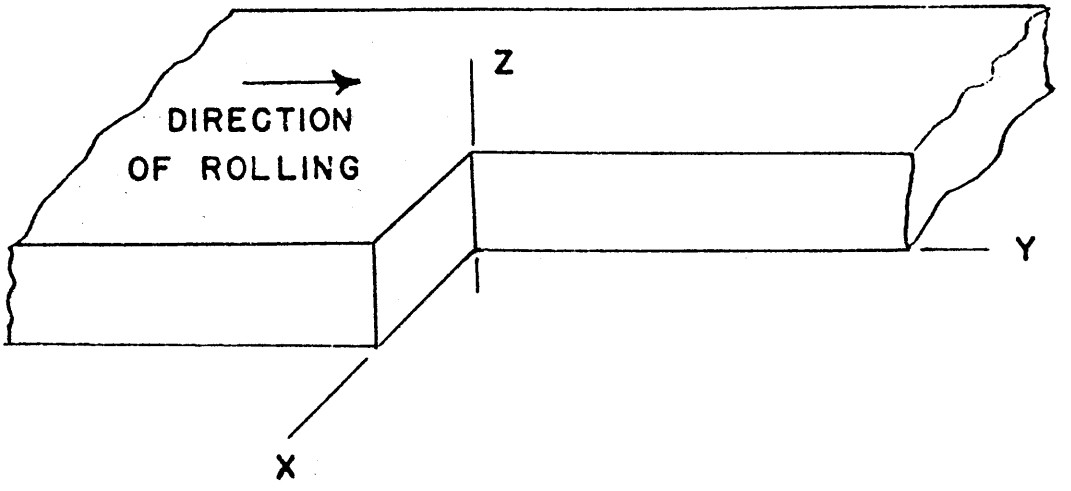

FIGURE 13. Orientation of reference axes in test specimens.

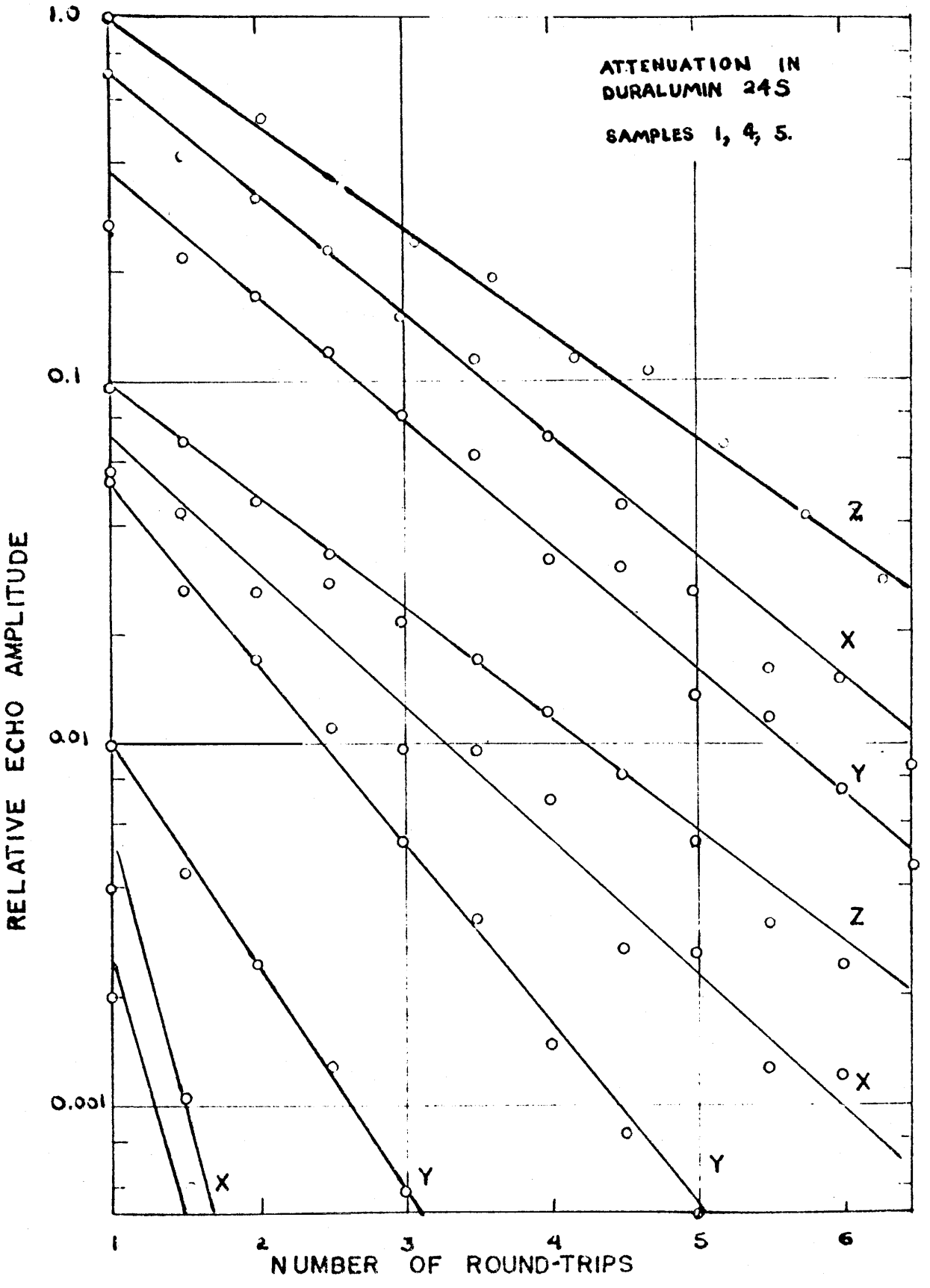

FIGURE 14. Unreduced data for duralumin samples.

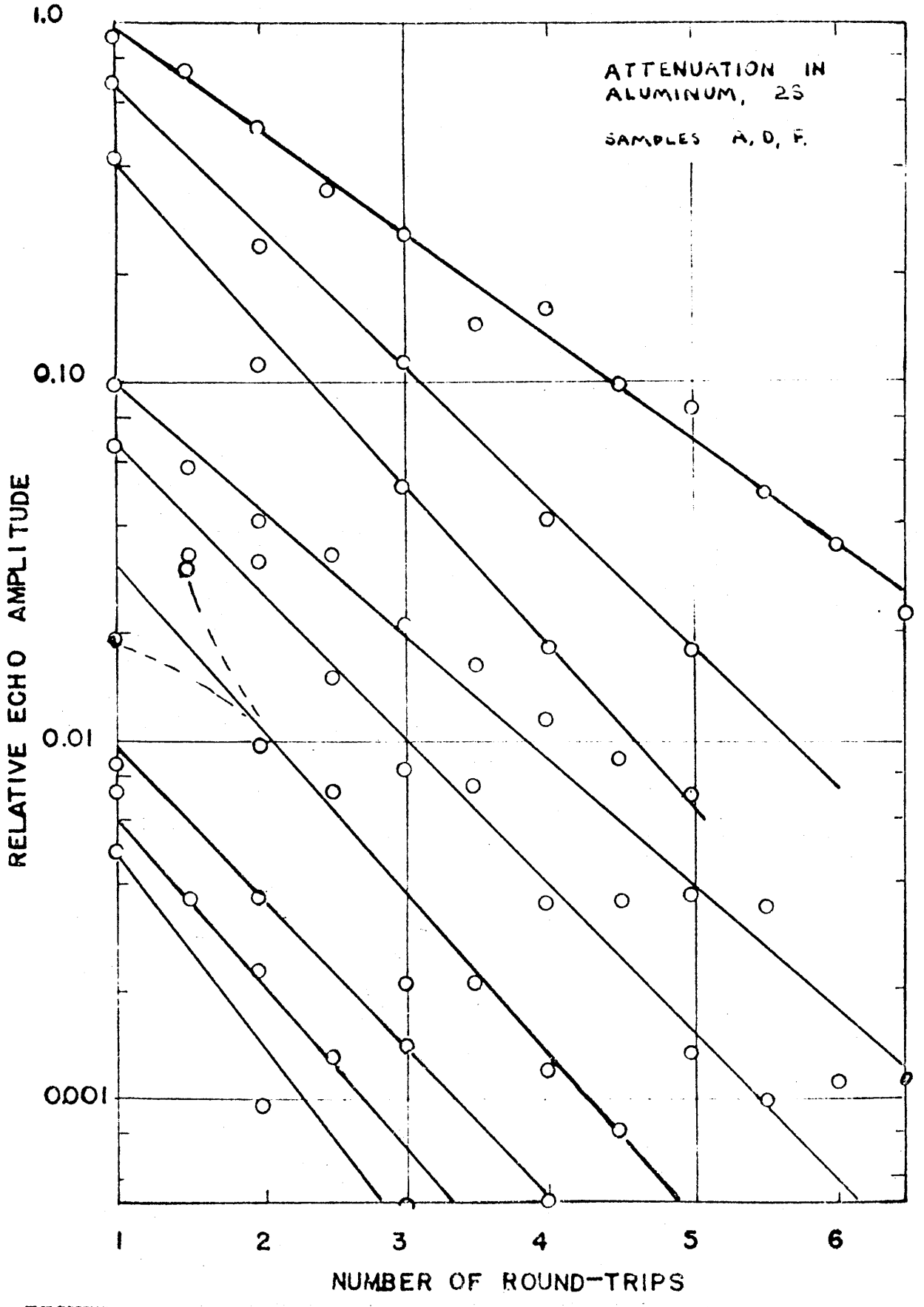

FIGURE 15. Unreduced data for pure aluminum samples.

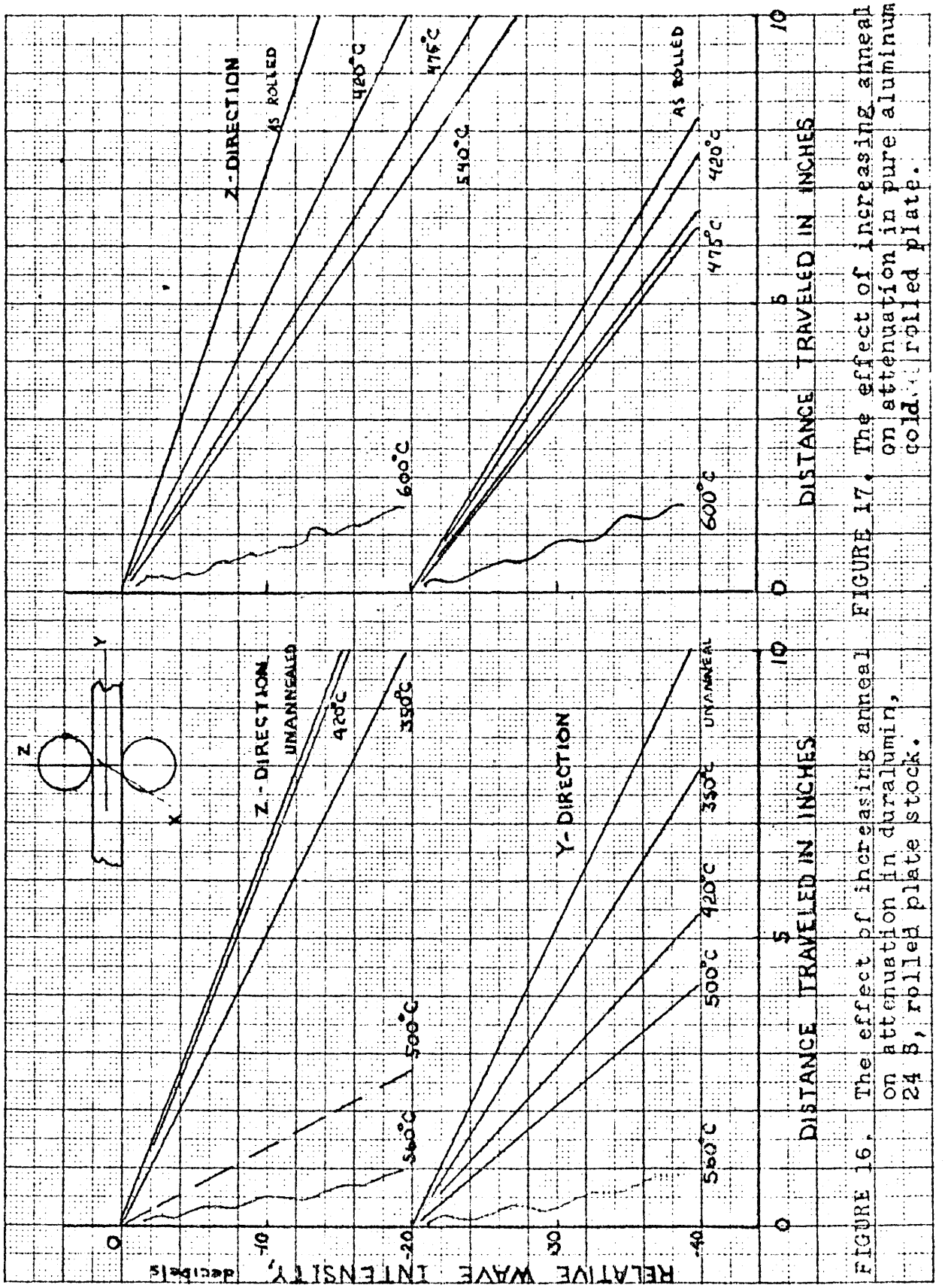

FIGURE 16. The effect of increasing anneal on attenuation in duralumin, 24 S, rolled plate stock.

FIGURE 17. The effect of increasing anneal on attenuation in pure aluminum gold, rolled plate.

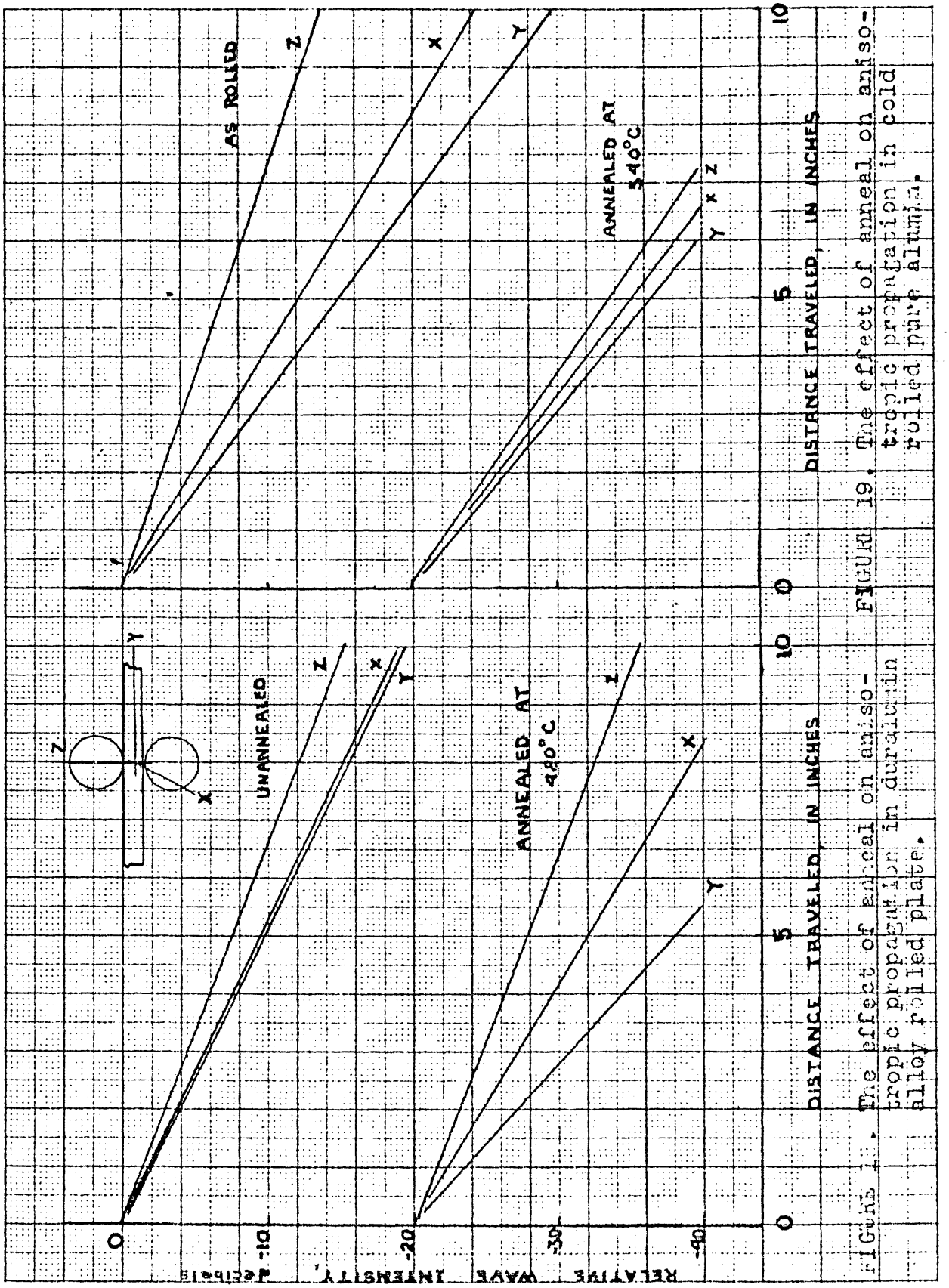

FIGURE 19. The effect of anneal on anisotropic propagation in duration in cold rolled pure aluminum alloy rolled plate.

FIGURE 20.

Oscillographic response with cold rolled 2S Al, unannealed (Sample A). Note the low attenuation and constant decrement.

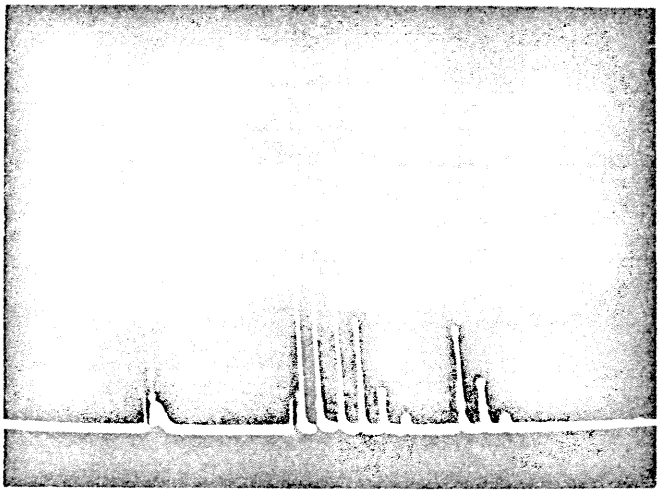

FIGURE 21.

Oscillographic response with same material as above, Fig. 20, but annealed at temperature 475°C for 25 minutes (Sample F, recrystallized grain size 0.04 mm)

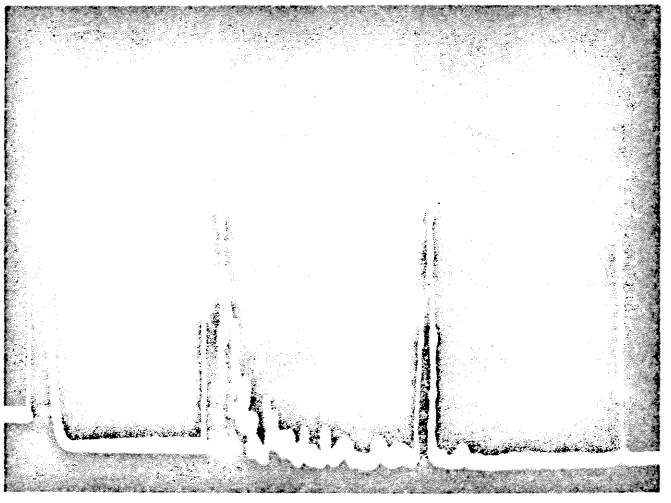

FIGURE 22.

Oscillographic response from same material as in Fig. 20, except it is annealed at 600°C for 25 minutes. Note the large grain-return, and complete absence of back surface reflections (Sample G, grain size 0.17 mm).

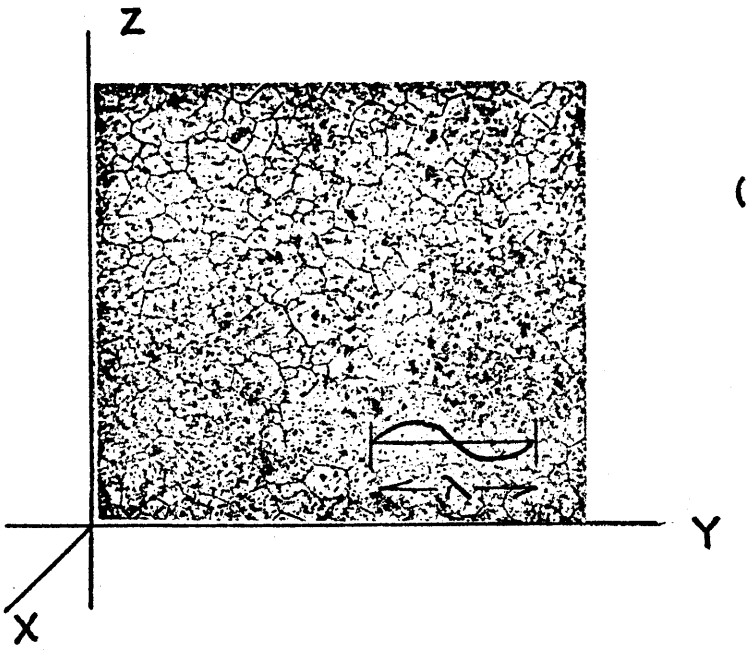

(a) Sample F, X100

D = 0.038 mm

Compare Figure 18.

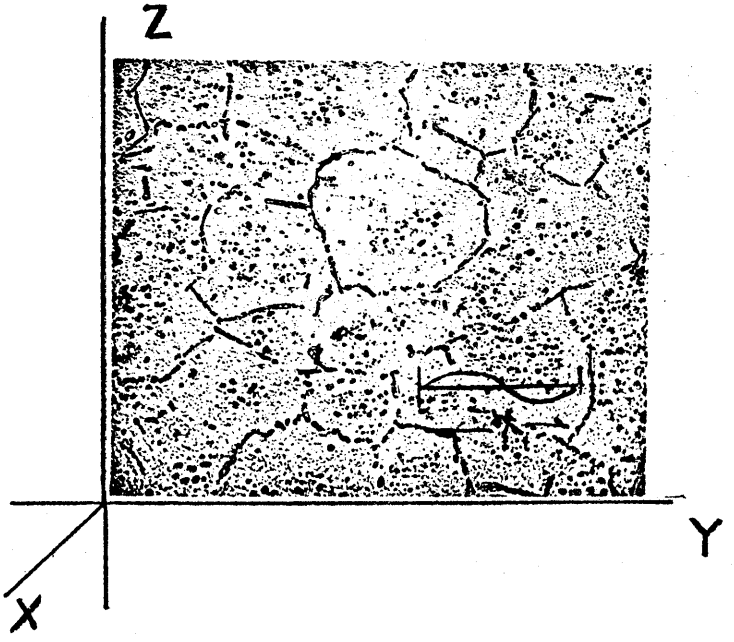

(b) Sample G, X100

D = 0.162 mm

Compare with Figures 19 and 22.

FIGURE 23. Micrographs of Aluminum samples showing structures.

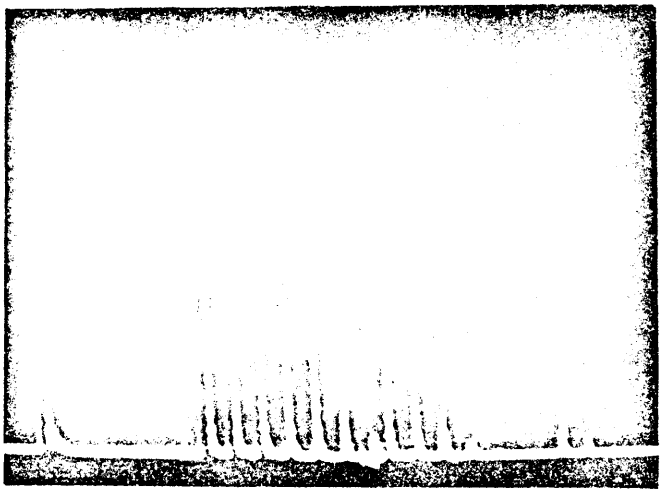

FIGURE 24.

Oscillographic response with Duralumin alloy 24S, as procured (Sample 1). Refer to Figure 28 a.

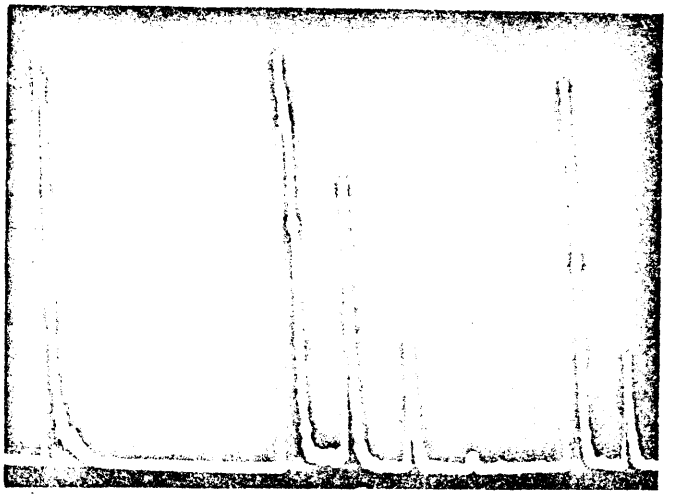

FIGURE 25 a.

Oscillographic response with Duralumin Sample 5, annealed at 500°C. Refer to Figure 28 c.

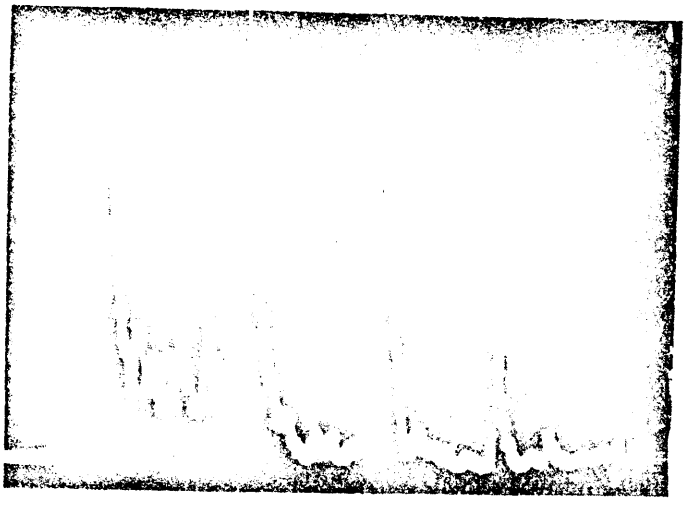

b

Same as (a) with sweep expanded and sensitivity increased to reveal internal echoes between major surface reflections.

FIGURE 26. Oscillographic response from duralumin sample no. 6.

Refer to Figure 28 d.

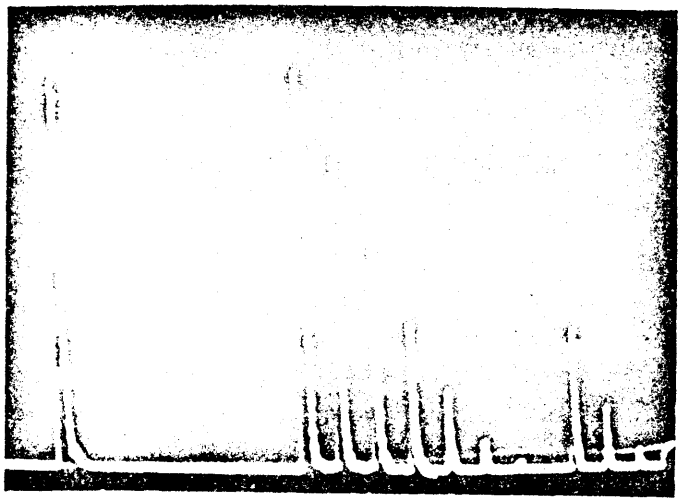

a

Oscillographic response for sample no. 4 with wave propagated in X-direction.

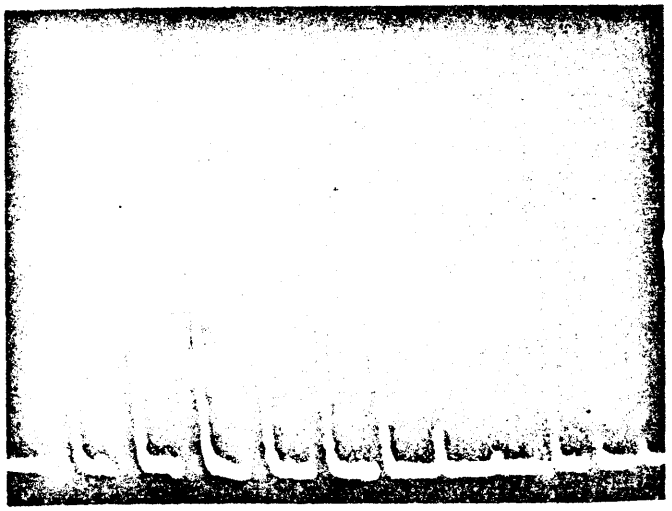

b

Same as above, (a), with sweep and sensi tivity expanded to re- veal echoes from grains.

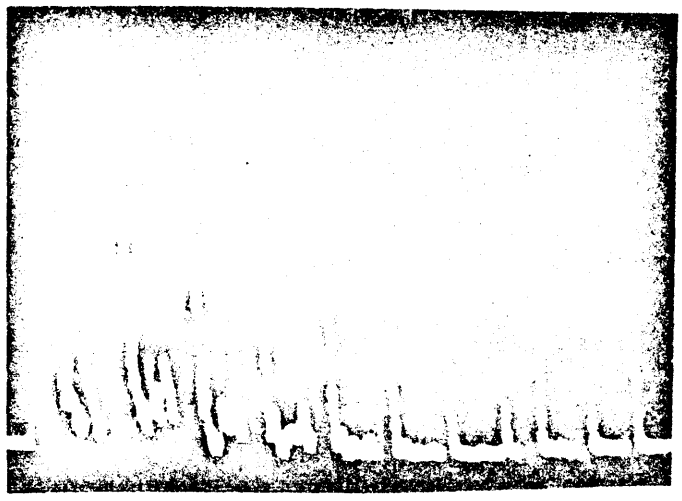

c

Same as (b), except sample is rotated 90°, with propagation along Z-direction. Note the increase of grain return.

FIGURE 27.

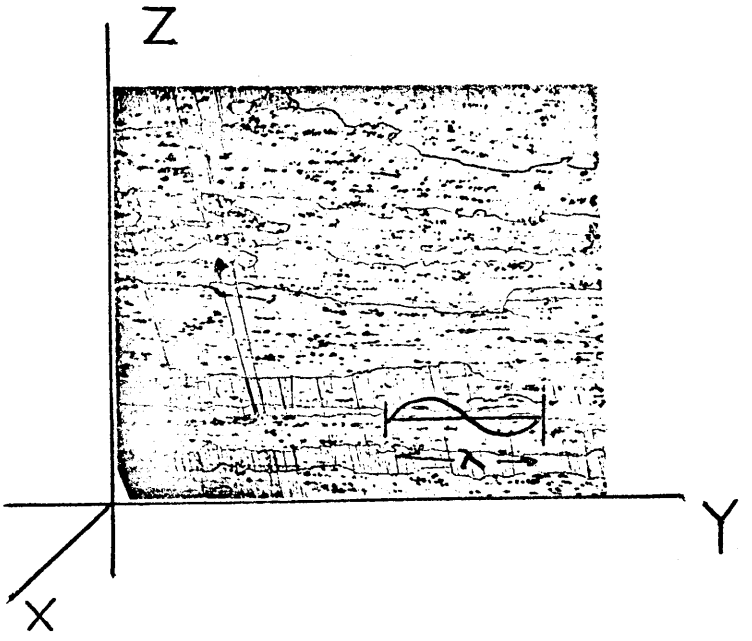

(a) Sample 1, X100

D = ?

Unannealed.

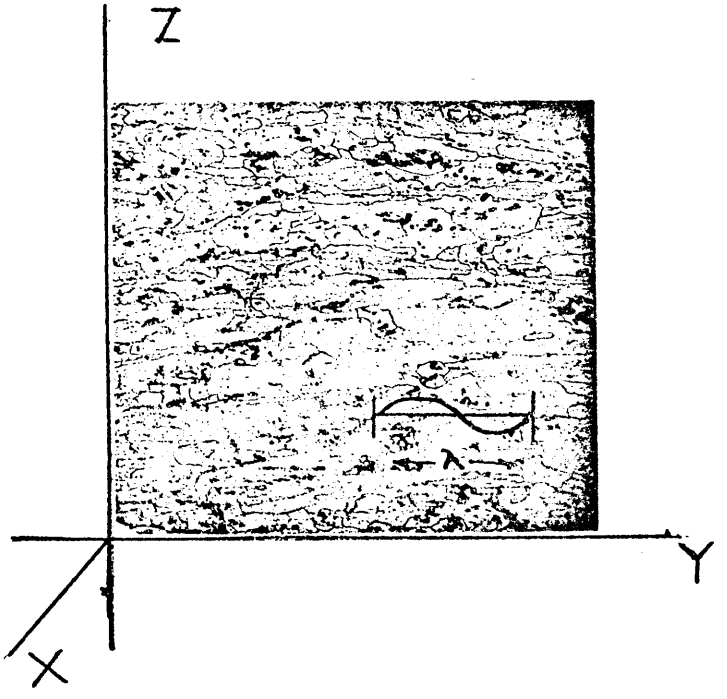

(b) Sample 4, X100

D = 0.042 mm

Annealed at 420°C, 30 minutes.

FIGURE 28. Micrographs of Duralumin samples. (Continued next page.)

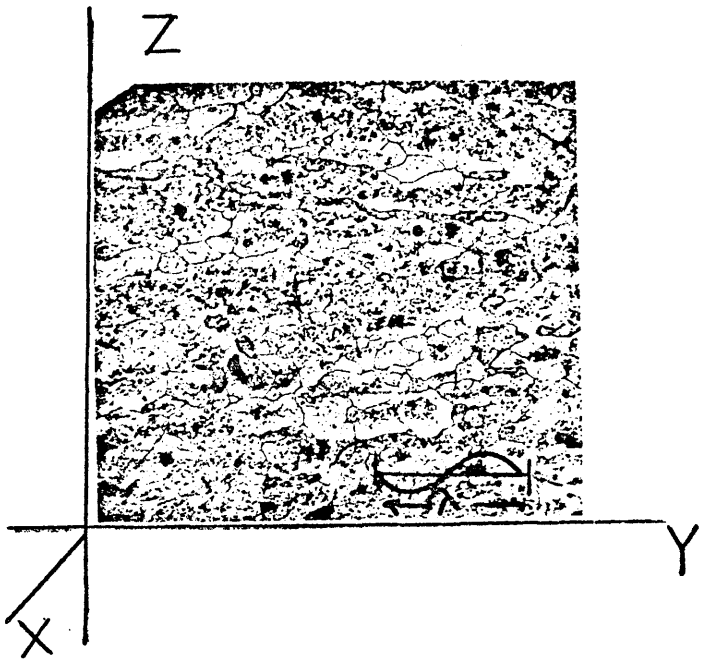

(c) Sample 5, X100

D = 0.048 mm

Annealed at 500°C, 30 minutes.

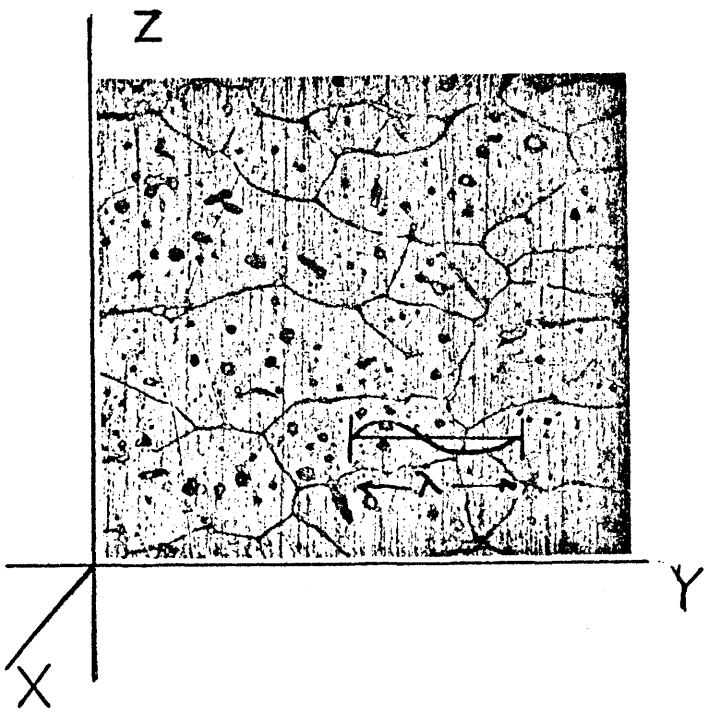

(d) Sample 6, X100

D = 0.151 mm

Annealed at 560°C, 30 minutes. Melting at the grain boundaries is Apparent. Ultrasonic propagation is extremely poor.

FIGURE 28. (Continued from previous page.)

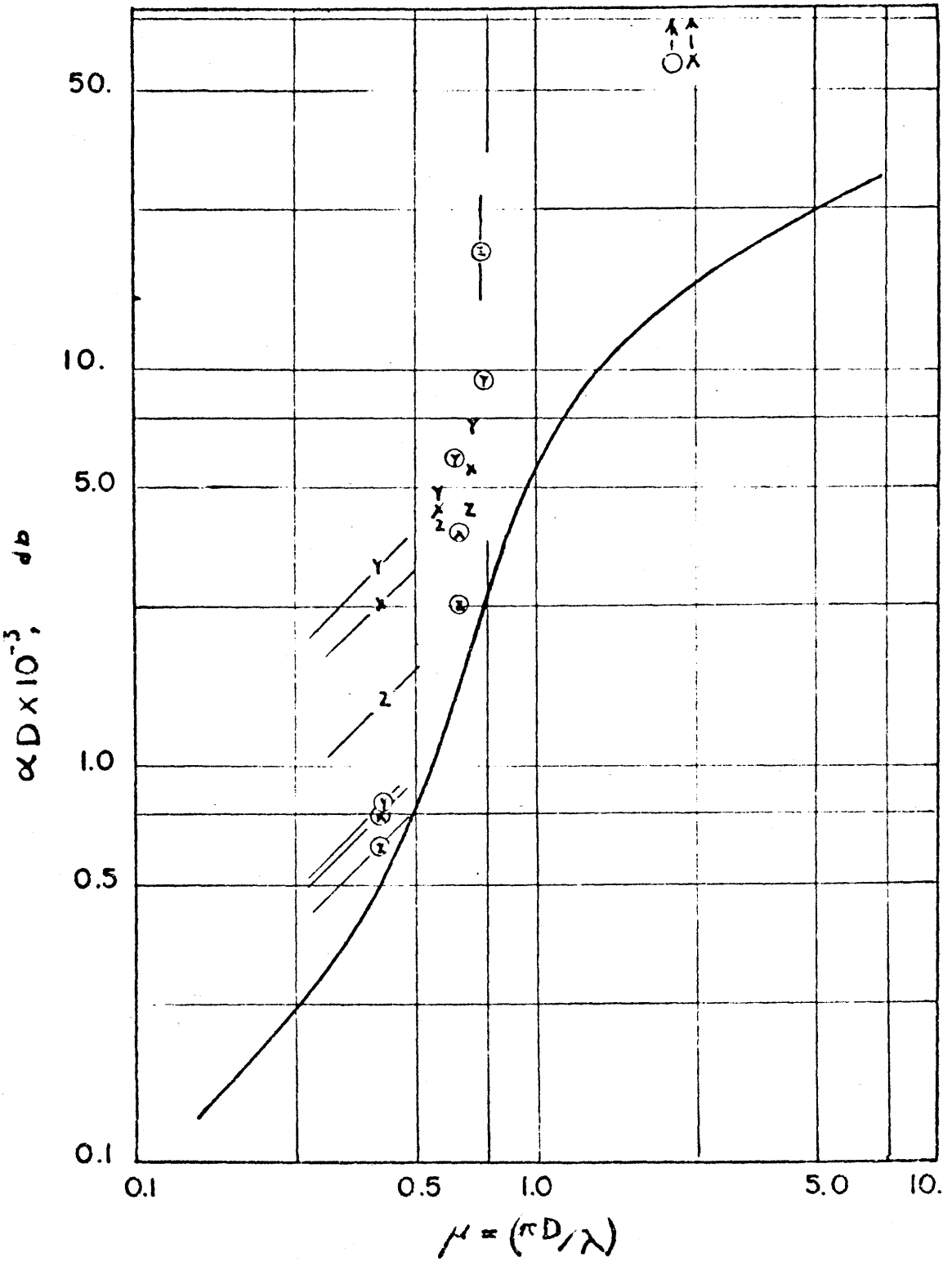

FIGURE 30. Plot of observed attenuations versus mean grain diameter on the dimensionless scales. The letters indicate the direction of propagation. The encircled points are for duralumin, the others for aluminum. The solid curve is the derived relation shown in Figure 3.

V. Conclusions and Recommendations.

On the basis of work previously reported and correlated in accordance with section II (b), above, the mechanism of ultrasonic attenuation below 80 mc/sec in polycrystalline metals may be described as (a), a hysteretic damping proportional to $1/\lambda$, and (b), a scattering by individual crystals dependent upon the ratio D/λ, the single crystal diameter to radiation wave length. Without further experimental evidence, a similar mechanism is predicted for still higher frequencies. It may be further concluded that in the case of low scattering materials, i.e., materials having crystals of low elastic anisotropy such as magnesium, or aluminum, the scattering component of the attenuation constant may be quantitatively described in terms of the scattering cross-section of a single particle, and the number of grains per unit length. Mason's formula is congruous with the theory presented here, for small values of the parameter $(\pi D/\lambda)$, and may be considered valid for $(\pi D/\lambda)$ less than 0.3, and approximate when $(\pi D/\lambda)$ is less than 1.0. However, it may be noted that for the first condition the scattering component of the attenuation is small compared to the hysteretic term for the case of aluminum (Figure 3), and Mason's formula becomes useful only in its range of approximation.

On the other hand, Roth's empirical formula gives a relation for only a particular combination of D and λ,

which cannot be generalized to a given range of $(\pi D/\lambda)$, or even to a given range of λ or D separately. The empirical equation itself (equation 6) appears to have little physical significance in explaining the mechanisms involved, though the data from which it was deduced are consistent with the theory developed here.

However, the preliminary experimental investigations of the author indicate that the results and theories advanced cannot be indiscriminately applied or extended without regard to the uniformity of grain dimensions in the material, or without regard to possible precipitation of second phases in alloys. Indeed, when a material exhibits anisotropic grain structure, the observed attenuation varies in a complicated manner depending upon the direction of propagation. Observing this fact, though lacking conclusive evidence of the fundamental processes involved, engineering applications are nevertheless apparent. Some conclusion may be made on the strain relief or grain elongation in a metal on the basis of the symmetry of ultrasonic propagation as an external engineering test, on an otherwise metallurgically unknown specimen. Considerably more work is needed before this can be made a practical or reliable test.

On the other hand, considerable qualitative knowledge of the grain size in aluminum can be deduced from the appearance of the echo response for an ultrasonic wave with wave length of a few tenths millimeter. Compare, for example, Figures 21 and 22 for grain structures shown in Figure 23,

(a) and (b), respectively; or compare Figures 24, 25, and 26 for structures shown in Figure 28, (a), (c), and (d) respectively. Considering the great difficulty experienced in revealing these structures metallographically, the possibility of estimating the same information ultrasonically is to be greatly appreciated.

The experimental work undertaken by the author with aluminum has been of an exploratory nature. Careful verification of the theory of attenuation requires metallurgical work of a quantity and quality beyond the scope of this thesis. Specifically, inorder to check more carefully the generality of the theoretical relation derived, it is recommended that investigations be made with frequency variable over such an extent as to cover completely the range

$$0.1 < \frac{\pi D}{\lambda} < 100$$

with a single grain diameter, and that the same coverage be made with as wide a range of grain diameter as possible, with a single material. That is, ideally it is desirable to cover the significant range of the parameter $(\pi D/\lambda)$ by both variable D with fixed λ, and by variable λ with fixed D. This will involve very careful preparation and determination of uniform and regular grain dimensions in individual specimens, with separate specimens ranging from very fine to very coarse grain in small steps.

References.

(1) Erdman, Donald C., Electrical Engineering. (1948) V 67. p.181.

(2) Firestone, F. A., Metal Progress. (1945) V 48, p.505.

(3) Desch, C.H., Sproule, D.O., and Dawson, W.J., Welding Journal. (1947) V 26, p.1.

(4) Struthers, F.W., and h.m. Trent, J.A.S.A. (1947) V 19. p.368.

(5) Boemmel, H. and R.V. Baud, Engineers Digest, (British Edition) (1947) V 8. p.128.

(6) Huntington, H.B., et al, Journal of the Franklin Institute. (1948) V 245. I, p.1, II, p.101.

(7) Roth, W. J. Appl. Phys. (1948) V 19. p.904.

(8) Mason, W.P. and H.J. McSkimin, J.A.S.A. (1947) V 19 p.464.

(9) Mason, W.P. and H.J. McSkimin, J. Appl. Phys. (1948) V 19. p.940.

(10) Mason, W.P. Piesoelectric Crystals and Their Applications to Ultrasonics. D. Van Nostrand Company. New York. (1950) p.245.

(11) Wegel, R.L. and H. Walther. Physics. (1935) V6. p.141.

(12) Rayleigh, Lord. Theory of Sound. McMillan and Co. London. (1878) V 2. p.138.

(13) Bergmann, L. Der Ultraschall. VDI*Verlag GMBH (1942) p.79, 180, 275.

(14) Morse, Philip M. Vibration and Sound. McGraw-Hill. New York. (1936) p.269, 257.

(15) Frankel, S. Radiation Laboratory Report 645-8, (1946).